Icarus **156**, 107–135 (2002)
doi:10.1006/icar.2001.6759, available online at http://www.idealibrary.com on IDEAL®

Alkali and Chlorine Photochemistry in a Volcanically Driven Atmosphere on Io

Julianne I. Moses

Lunar and Planetary Institute, 3600 Bay Area Boulevard, Houston, Texas 77058-1113
E-mail: moses@lpi.usra.edu

Mikhail Yu. Zolotov

Department of Earth and Planetary Sciences, Washington University CB1169, One Brookings Drive, St. Louis, Missouri 63130-1899

and

Bruce Fegley, Jr.

Department of Earth and Planetary Sciences, Planetary Chemistry Laboratory, McDonnell Center for the Space Sciences, Washington University CB1169, One Brookings Drive, St. Louis, Missouri 63130-1899

Received November 15, 2000; revised September 17, 2001

Observations of the Io plasma torus and neutral clouds indicate that the extended ionian atmosphere must contain sodium, potassium, and chlorine in atomic and/or molecular form. Models that consider sublimation of pure sulfur dioxide frost as the sole mechanism for generating an atmosphere on Io cannot explain the presence of alkali and halogen species in the atmosphere—active volcanoes or surface sputtering must also be considered, or the alkali and halide species must be discharged along with the SO_2 as the frost sublimates. To determine how volcanic outgassing can affect the chemistry of Io's atmosphere, we have developed a one-dimensional photochemical model in which active volcanoes release a rich suite of S-, O-, Na-, K-, and Cl-bearing vapor and in which photolysis, chemical reactions, condensation, and vertical eddy and molecular diffusion affect the subsequent evolution of the volcanic gases. Observations of Pele plume constituents, along with thermochemical equilibrium calculations of the composition of volcanic gases exsolved from high-temperature silicate magmas on Io, are used to constrain the composition of the volcanic vapor. We find that NaCl, Na, Cl, KCl, and K will be the dominant alkali and chlorine gases in atmospheres generated from Pele-like plume eruptions on Io. Although the relative abundances of these species will depend on uncertain model parameters and initial conditions, these five species remain dominant for a wide variety of realistic conditions. Other sodium and chlorine molecules such as NaS, NaO, Na_2, NaS_2, NaO_2, NaOS, $NaSO_2$, SCl, ClO, Cl_2, S_2Cl, and SO_2Cl_2 will be only minor constituents in the ionian atmosphere because of their low volcanic emission rates and their efficient photochemical destruction mechanisms. Our modeling has implications for the general appearance, properties, and variability of the neutral sodium clouds and jets observed near Io. The neutral NaCl molecules present at high altitudes in atmospheres generated by active volcanoes might provide the NaX^+ ion needed to help explain the morphology of the high-velocity sodium "stream" feature observed near Io. © 2002 Elsevier Science (USA)

Key Words: **Io; photochemistry; atmospheres, composition; volcanism; geochemistry; alkalis; halogens.**

1. INTRODUCTION

Io's tenuous and spatially heterogeneous atmosphere appears to be composed predominantly of sulfur dioxide, with smaller amounts of SO, S, O, Na, K, Cl, and (perhaps) H being observed in Io's near-surface and/or extended atmosphere (see Retherford *et al*. 2000; McGrath *et al*. 2000; Trafton 2000; Roesler *et al*. 1999, and the reviews of Spencer and Schneider 1996 and Lellouch 1996). Observations of the Io plasma torus provide further evidence, albeit indirect, for these constituents being present—sulfur dioxide and its dissociation products must be major components of the atmosphere, and minor amounts of the alkali elements sodium and potassium in atomic and/or molecular form must also be present to continuously resupply the torus and neutral clouds (e.g., Brown 1974, Trafton 1975, Thomas 1992, Spencer and Schneider 1996). The recent discovery of Cl^+ and Cl^{++} in the Io torus (Küppers and Schneider 2000, Schneider *et al*. 2000, Feldman *et al*. 2000) and neutral Cl in the aurora (Retherford *et al*. 2000) implies that chlorine must also exist in Io's atmosphere, but the exact form (i.e., molecular or atomic) of the dominant chlorine component is unknown. The reported Cl^+ and Cl^{++} number densities indicate that chlorine has roughly the same abundance as sodium in the torus (e.g., Schneider *et al*. 2000); however, spatial and/or temporal variability of the atmospheric Na/Cl ratio is possible on geochemical

0019-1035/02 $35.00

grounds and should be considered. The discovery of diatomic sulfur (S_2) within an active volcanic plume at Pele (Spencer *et al*. 2000) constitutes the first direct detection of a near-surface molecular constituent other than SO_2 and its dissociation product SO. Although the ultimate source of volatiles for Io's surface and atmosphere is extensive volcanism driven by tidal heating, the relative importance of frost sublimation, surface sputtering, and active volcanism in generating and maintaining Io's atmosphere is not well understood.

Most theoretical models have focused on atmospheres that are in equilibrium with surface or subsurface SO_2 frost deposits (Kumar 1980, 1982, 1984, Fanale *et al*. 1982, Matson and Nash 1983, Summers and Strobel 1996, Wong and Johnson 1996a, Wong and Smyth 2000). The photochemistry of such a sublimation-driven SO_2 atmosphere on Io is relatively straightforward, with SO_2, SO, O, S, and O_2 being the only important photochemical products (e.g., Kumar 1982, Summers and Strobel 1996, Wong and Johnson 1996a). However, to explain the presence of the photochemically reactive S_2 molecule or alkali and halogen species in Io's atmosphere, photochemical models must also consider sputtering of surface deposits or emission from active volcanoes (e.g., Kumar 1985, Summers and Strobel 1996, Wong and Smyth 2000, Moses *et al*. 2002). Several recent observations indicate that active volcanoes might play a larger role in controlling atmospheric properties than was previously thought. The apparent patchiness of SO_2 vapor across Io's surface, the correlation of observed atomic and molecular emission features with known volcanic centers on Io, and the observed red-shifted and broadened shape of the SO_2 and SO lines at millimeter wavelengths all suggest that volcanoes are important atmospheric drivers (e.g., Lellouch *et al*. 1990, 1992, 1994, 1996; Ballester *et al*. 1990, 1994; Sartoretti *et al*. 1994, 1996; Lellouch 1996; McEwen *et al*. 1998; Geissler *et al*. 1999; Hendrix *et al*. 1999; Bouchez *et al*. 2000; and McGrath *et al*. 2000; see also the theoretical models of Ingersoll 1989, Moreno *et al*. 1991, Strobel and Wolven 2001). In addition, theoretical modeling of the equilibrium chemistry of ionian volcanic vapors suggests that a variety of S-, O-, Na-, K-, and Cl-bearing gases may be emitted from high-temperature silicate magmas on Io (see Zolotov and Fegley 1998a, 1998b, 1999, 2000; Fegley and Zolotov 2000). These volcanic gases can alter the composition and chemistry of Io's atmosphere (e.g., Moses *et al*. 2002).

To determine how active volcanism might influence Io's atmospheric composition, we have developed a simple one-dimensional photochemical model that traces the fate of sulfur, oxygen, sodium, potassium, and chlorine gases emitted from Pele-type volcanic plume eruptions at Io's surface. Thermochemical equilibrium calculations based on the work of Zolotov and Fegley (2000) and Fegley and Zolotov (2000), along with the Pele observations of McGrath *et al*. (2000) and Spencer *et al*. (2000), are used to constrain the initial composition of the volcanic vapor and thus the initial and boundary conditions of the photochemical model. Chlorine and potassium compounds have never before been included in photochemical models. Sodium-bearing gases have been considered in previous models (e.g., Kumar 1985, Summers 1985, Summers and Strobel 1996, Wong and Smyth 2000), but only in a somewhat *ad hoc* manner, with the modelers simply fixing the mixing ratios or upward fluxes of sodium-containing species (sometimes without regard to realistic descriptions of their possible sources or source strengths). By considering an active volcanic source, we provide a more self-consistent description of how sodium-bearing gases could be released along with a full suite of potassium, chlorine, sulfur, and oxygen vapors. We find that the photochemistry of an atmosphere generated by Pele-type plumes is considerably more complex than that of an atmosphere generated by pure SO_2 frost sublimation. The number of photochemical products is increased, the relative importance of the different products changes, and alkali and halogen interactions become important.

In this paper, we focus on the photochemistry of neutral alkali and chlorine species released from a continuous Pele-like plume eruption on Io. The results regarding neutral sulfur and oxygen species are discussed in a companion paper in this volume (Moses *et al*. 2002; hereafter called Paper 1). We identify the important production and loss schemes for the major sodium-, potassium-, and chlorine-bearing volcanic volatiles, and we determine the time scales for the photochemical evolution of these vapors once the volcanic sources are turned on or off. We also discuss the implications of our modeling for the observed composition of the atmosphere, surface, and neutral clouds.

2. PHOTOCHEMICAL MODEL

Using the Caltech/JPL chemical kinetics and diffusion code (e.g., Allen *et al*. 1981, Yung *et al*. 1984, Summers 1985), we solve the coupled one-dimensional continuity equations in spherical geometry for all of the proposed constituents in Io's atmosphere. Vertical transport is assumed to be controlled by eddy and molecular diffusion, and the eddy diffusion coefficient in our standard model is assumed to be $K_E = 10^9$ cm^2 s^{-1}, independent of altitude (see Paper 1 for further discussion). The solar zenith angle is fixed at 60°, and solar flux values relevant to periods of low solar activity (sunspot minimum) are used throughout (see Mills 1998). Both steady-state and time-variable solutions to the continuity equations are considered. Although the model is designed to represent average conditions within a relatively broad quasi-hydrostatic area surrounding a major plume eruption on Io, our neglect of plume dynamics and horizontal transport away from the vent will prevent our model from representing the true state of a volcanically generated atmosphere (see Ingersoll 1989, Moreno *et al*. 1991, Austin and Goldstein 1996), and our results should be considered as first-order predictions of the possible photochemical processing of different volcanic gases on Io.

Consistent with Summers and Strobel (1996), we assume maximum "limiting" flux boundary conditions at the top boundary (∼600 km) for all species in the model (except SO_2) to simulate efficient atmospheric escape. Unlike previous models, we

assume that a volcanic source continuously introduces vapors at the lower boundary (Io's surface). Thermochemical equilibrium calculations based on Zolotov and Fegley (2000) and Fegley and Zolotov (2000) are used to specify the mixing ratios of the volcanic vapors from a Pele-like plume eruption (see Paper 1). Fixed mixing ratio boundary conditions are then used at the lower boundary for those volcanic species. A full description of the photochemical model and a more complete discussion of our adopted boundary conditions are presented in Paper 1.

Three background model atmospheres are considered in this paper. For our standard model, we assume a surface atmospheric pressure intermediate between the high-density and low-density cases of Summers and Strobel (1996). The surface pressure and total atmospheric column density in this "moderate-density" model are 2.1 nbars and 1.1×10^{17} cm^{-2}, respectively, and the temperature profile is modified from the 3.5×10^{-9} bar model of Strobel *et al*. (1994). Temperatures range from 113 K at the surface to ~1700 K at 600 km altitude (see Paper 1). We also examine the results for models with much higher and lower surface densities. The "high-density" model is similar to the high-density case of Summers and Strobel (1996) and has a surface pressure of 18 nbars and a total atmospheric column density of 9.6×10^{17} cm^{-2}. The "low-density" model has a surface pressure of 0.37 nbar and a total atmospheric column density of 2.0×10^{16} cm^{-2}. The exobase altitudes for the low-, moderate-, and high-density models are 370, 616, and 526 km, respectively (see Paper 1 for more details).

For our standard model, we assume that the volcanic vapors being emitted on Io consist of gases that have been in contact with high-temperature silicate magma. The relative elemental composition for the volcanic gases is assumed to be 1.521/1.0/0.05/0.05/0.005 for O/S/Na/Cl/K. We also examine the sensitivity of the results to different assumptions about the elemental composition. For an assumed vent pressure of 6.9×10^{-6} bar and magma temperature of 1440 K (which Zolotov and Fegley 2000 determine are relevant to a Pele-like eruption), our thermochemical equilibrium calculations suggest that the exsolved volcanic vapors are composed predominantly of SO_2, S_2, and SO (see Zolotov and Fegley 2000 and Paper 1), with the major alkali and halogen species being NaCl, Na, KCl, Cl, and K (see Fegley and Zolotov 2000). Table I lists the Na-, Cl-, and K-bearing species that have been included in our photochemical and thermochemical models; the column labeled "Initial" describes the abundances (relative to SO_2) derived from the thermochemical equilibrium calculations (see Zolotov and Fegley 2000 and Paper 1 for more details). The photodissociation and gas-phase kinetics reactions for the chlorine, potassium, and sodium species are listed in the Appendix. Condensation of NaCl and KCl are very important in the model; a description of our method for including condensation is also presented in the Appendix.

The adopted O/S ratio for the volcanic gases in our model is strictly only appropriate for Pele-type eruptions that contain

TABLE I
Abundance Relative to SO_2

Constituent	Initial	Moderate density case	High density case	Low density case
Cl	1.73×10^{-4}	7.03×10^{-3}	2.99×10^{-3}	7.90×10^{-3}
Cl_2	1.14×10^{-10}	1.40×10^{-10}	8.35×10^{-11}	1.32×10^{-10}
ClO	7.43×10^{-12}	3.41×10^{-10}	7.99×10^{-12}	1.48×10^{-10}
ClOO	—	9.12×10^{-16}	1.07×10^{-15}	2.98×10^{-16}
OClO	—	1.30×10^{-30}	8.59×10^{-31}	1.41×10^{-31}
Cl_2O	4.46×10^{-22}	1.43×10^{-22}	1.07×10^{-22}	2.35×10^{-22}
Cl_2O_2	—	7.81×10^{-29}	1.61×10^{-28}	5.59×10^{-30}
SCl	9.40×10^{-9}	3.00×10^{-9}	1.19×10^{-9}	2.35×10^{-9}
SCl_2	1.35×10^{-13}	2.06×10^{-14}	1.67×10^{-14}	3.03×10^{-14}
S_2Cl	8.65×10^{-10}	4.88×10^{-9}	2.95×10^{-7}	1.21×10^{-9}
S_2Cl_2	1.20×10^{-17}	1.81×10^{-18}	1.47×10^{-18}	2.59×10^{-18}
OSCl	—	3.73×10^{-9}	2.55×10^{-10}	3.86×10^{-9}
$ClSO_2$	—	1.79×10^{-8}	2.18×10^{-9}	1.36×10^{-8}
$SOCl_2$	4.35×10^{-15}	—	—	—
SO_2Cl_2	7.13×10^{-22}	1.52×10^{-13}	2.12×10^{-13}	2.04×10^{-14}
Na	6.84×10^{-3}	1.30×10^{-2}	9.41×10^{-3}	1.36×10^{-2}
Na_2	7.83×10^{-12}	3.31×10^{-8}	1.94×10^{-5}	1.81×10^{-10}
NaO	3.37×10^{-9}	8.56×10^{-10}	7.71×10^{-10}	9.50×10^{-10}
NaO_2	—	4.81×10^{-13}	5.81×10^{-12}	4.43×10^{-14}
NaO_3	—	5.18×10^{-20}	2.33×10^{-18}	8.53×10^{-21}
Na_2O	7.65×10^{-15}	5.02×10^{-15}	4.01×10^{-15}	6.05×10^{-15}
NaS	—	2.87×10^{-8}	7.75×10^{-7}	1.95×10^{-9}
NaS_2	—	9.82×10^{-7}	7.19×10^{-5}	3.94×10^{-8}
Na_2S	—	2.03×10^{-15}	8.17×10^{-12}	2.36×10^{-18}
NaOS	—	6.33×10^{-7}	3.79×10^{-5}	3.38×10^{-8}
$NaSO_2$	—	6.72×10^{-6}	3.37×10^{-4}	2.59×10^{-7}
Na_2SO_4	8.88×10^{-14}	8.29×10^{-14}	8.80×10^{-14}	7.23×10^{-14}
NaCl	6.13×10^{-2}	5.28×10^{-2}	5.46×10^{-2}	5.26×10^{-2}
$NaCl_{(con)}$	—	3.22×10^{-3}	4.11×10^{-3}	2.93×10^{-3}
$(NaCl)_2$	9.69×10^{-8}	1.03×10^{-7}	1.79×10^{-6}	8.19×10^{-8}
$(NaCl)_3$	2.30×10^{-14}	4.37×10^{-14}	5.59×10^{-11}	1.81×10^{-14}
K	1.50×10^{-4}	9.01×10^{-4}	4.56×10^{-4}	9.78×10^{-4}
K_2	1.67×10^{-15}	2.46×10^{-15}	1.62×10^{-13}	9.56×10^{-16}
KO	6.24×10^{-11}	1.10×10^{-10}	1.52×10^{-10}	8.51×10^{-11}
KO_2	—	4.65×10^{-14}	3.93×10^{-13}	3.65×10^{-15}
K_2O	2.15×10^{-17}	1.83×10^{-17}	2.62×10^{-17}	1.78×10^{-17}
KS	1.91×10^{-7}	3.57×10^{-8}	2.75×10^{-7}	4.73×10^{-8}
KS_2	—	1.19×10^{-7}	8.39×10^{-6}	4.15×10^{-9}
K_2S	2.37×10^{-14}	1.10×10^{-14}	1.48×10^{-14}	1.58×10^{-14}
KSO_2	—	7.71×10^{-7}	4.30×10^{-5}	2.37×10^{-8}
K_2SO_4	7.41×10^{-16}	6.80×10^{-16}	7.33×10^{-16}	5.76×10^{-16}
KCl	6.67×10^{-3}	5.74×10^{-3}	6.07×10^{-3}	5.52×10^{-3}
$KCl_{(con)}$	—	2.44×10^{-4}	3.21×10^{-4}	2.12×10^{-4}
$(KCl)_2$	9.65×10^{-10}	1.04×10^{-9}	2.21×10^{-8}	7.74×10^{-10}
KNa	2.89×10^{-13}	2.01×10^{-13}	4.34×10^{-12}	1.63×10^{-13}

Note. Only neutral species containing alkali or halogen elements are included in the table. Mixing ratios represent the column density of the constituent divided by the column density of SO_2. Mixing ratios of "—" indicate that the constituent was not included in either the thermochemical equilibrium calculations (second column) or the photochemical model (last three columns), and the subscript (*con*) refers to the condensed phase. The SO_2 column density is 8.35×10^{16} cm^{-2} for the moderate-density case, 7.37×10^{17} cm^{-2} for the high-density case, and 1.48×10^{16} cm^{-2} for the low-density case. Sulfur dioxide is initially 77.2% of all the volcanic vapors.

relatively reduced gases that were exsolved from high-temperature silicate magmas (i.e., eruptions in which S_2 is present as the second-most abundant vapor other than SO_2; see Zolotov and Fegley 2000). Fegley and Zolotov (2000) show that volcanic gases emitted at lower temperatures and pressures could contain sodium, potassium, and chlorine predominantly in the form of NaCl and KCl vapor, and more oxidized volcanoes could emit gases that have much higher SO_2/S_2 ratios than Pele-type volcanoes. Photochemical processes will still cause NaCl, KCl, Na, Cl, and K to be the dominant atmospheric gases from such eruptions, but the relative proportions may change from the results discussed below.

3. MODEL RESULTS AND DISCUSSION

Figure 1 shows the solutions to the steady-state continuity equations for the major atmospheric constituents in our standard moderate-density model. Although ion chemistry and neutral sulfur and oxygen chemistry are not discussed in this paper, the concentrations of all the important atmospheric species are included in Fig. 1 to show how alkali and halogen concentrations compare with other constituents. Table I lists the column-integrated mixing ratios for all the alkali and chlorine species in the model. Note that photochemistry has altered the initial volcanic composition. For example, the NaCl and KCl abundances have decreased slightly relative to the initial volcanic composition, while the abundances of Na, K, and Cl have increased slightly.

The alkali species in our model are produced predominantly from volcanic NaCl and KCl, with a lesser contribution from Na, K, and KS. The chlorine species also derive mainly from NaCl and KCl, with some contribution from Cl, SCl, and Cl_2. The major photochemical pathways for producing and destroying sodium and chlorine species in our moderate-density model are shown in Figs. 2 and 3. The important photochemical pathways for potassium species are very similar to those for sodium, and a separate potassium figure is not presented. Because of a lack of laboratory data on the reaction rates and mechanisms of alkali and halogen species with sulfur species, the results in this section should be regarded as speculative.

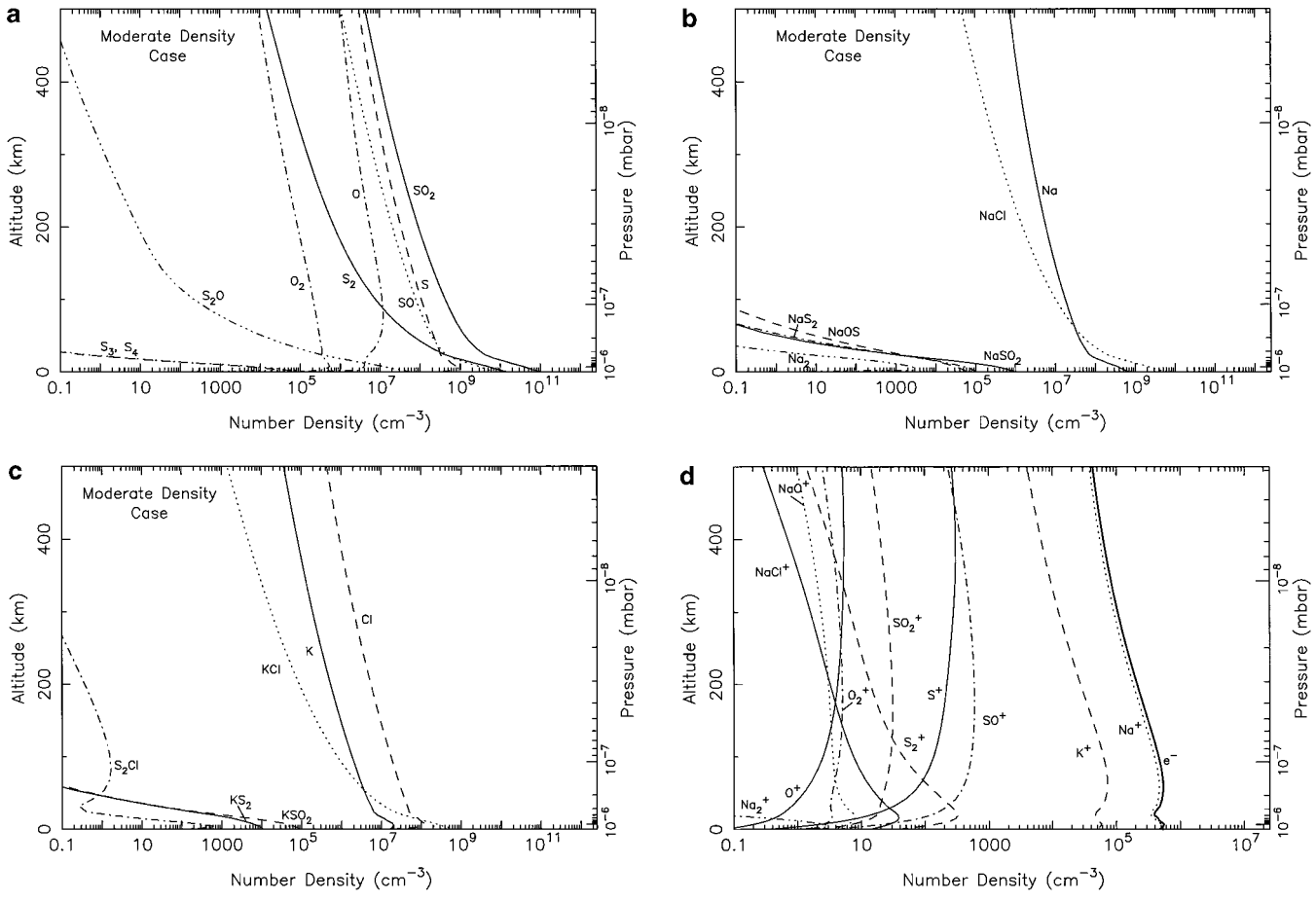

FIG. 1. The concentrations of several important atmospheric constituents in our standard moderate-density model (e.g., 2.1 nanobar surface pressure, SO_2 column density 8.4×10^{16} cm^{-2}, $K_E = 10^9$ cm^2 s^{-1}) as a function of altitude and pressure: (a) sulfur and oxygen species, (b) sodium species, (c) potassium and chlorine species, and (d) ions. Ion densities are approximate due to our neglect of photoelectron ionization and impact ionization from torus electrons and ions.

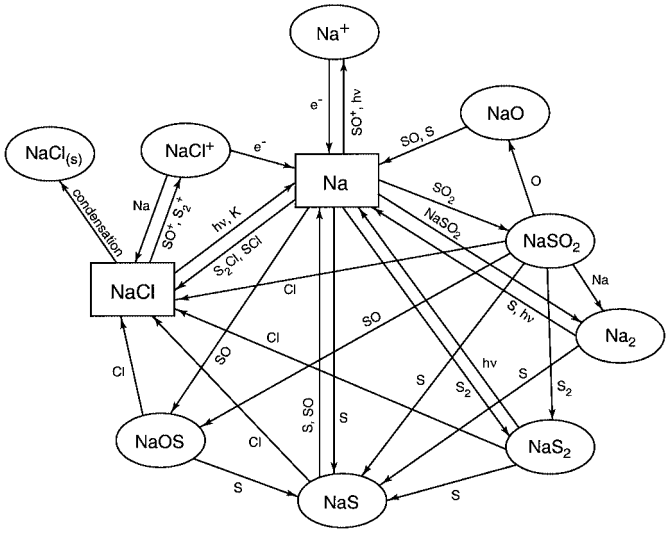

FIG. 2. A schematic diagram illustrating the important reaction pathways for sodium species in our standard moderate-density model. Important "parent" volcanic gases are outlined as rectangles, and "daughter" products are outlined as ovals. The symbol hν corresponds to an ultraviolet photon, the subscript (s) refers to the solid phase, and e^- refers to electrons. The important pathways for potassium species are similar to those for sodium.

3.1. Sodium Photochemistry

Sodium chloride vapor is the dominant reservoir for both sodium and chlorine at thermochemical equilibrium in an ionian volcanic gas with Na $\geq$ Cl (Fegley and Zolotov 2000; see Table I). In our standard model, NaCl is lost mainly by photodissociation (reaction R50: $NaCl + h\nu \rightarrow Na + Cl$) and by condensation onto plume dust particles (or other atmospheric aerosols), as is described in Table II. The absolute abundances for vapor and solid NaCl listed in Table I should not be taken too seriously, as the results are very sensitive to details concerning the efficiency of condensation (see the Appendix and Section 4.3). However, for all reasonable assumptions about the condensation rate, volcanic NaCl is a major "parent" gas for both sodium and chlorine photochemistry. In our moderate-density model, photolysis (i.e., reaction R50) accounts for $\sim$52% of the total column loss rate for NaCl, and condensation accounts for $\sim$48% (see Table II). Because of interest in alkali metal chemistry in the Earth's stratosphere and mesosphere, the photoabsorption cross sections for NaCl have been measured in the laboratory; we use the cross sections of Silver *et al.* (1986).

Sodium chloride vapor is not efficiently recycled in our moderate-density model, and its loss rate greatly exceeds its production rate (see Table II). If volcanic sources were eliminated, NaCl would be quickly depleted from Io's atmosphere unless efficient sputtering from surface salt deposits allowed NaCl vapor to be resupplied. The dominant NaCl production mechanism in our model is reaction R372 ($Cl + NaS \rightarrow NaCl + S$; 28% of the total column production rate), followed by reaction R373 ($Cl + NaS_2 \rightarrow NaCl + S_2$; 26.5% of total production), reaction R377 ($Cl + NaSO_2 \rightarrow NaCl + SO_2$; 11.8% of total production), reaction R455 ($S_2Cl + Na \rightarrow NaCl + S_2$; 11.5% of the total production), and reaction R445 ($SCl + Na \rightarrow NaCl + S$; 9.7% of total production). Although all of the above reactions are speculative, it is unlikely that their rate coefficients could be much higher than we have estimated. Therefore, we are confident in our conclusion that NaCl is not efficiently recycled and that NaCl vapor should be more apparent during active volcanic periods on Io.

Unlike NaCl, atomic sodium is produced much more readily than it is destroyed photochemically (see Table II). The predominant production mechanism for Na is NaCl photolysis (reaction R50), with minor (i.e., less than 1%) contributions from reaction R484 ($NaCl + K \rightarrow KCl + Na$), reaction R338 ($SO + NaS \rightarrow S_2O + Na$), and reaction R251 ($S + NaS \rightarrow Na + S_2$).

Although Na is not easily destroyed by photochemical means, its destruction leads to the formation of many interesting sodium compounds (see Fig. 2). The dominant photochemical loss process for Na in our moderate-density model is reaction R342 ($SO_2 + Na + M \rightarrow NaSO_2 + M$; $\sim$70% of the total column destruction rate of Na). Both the low- and high-pressure limiting rate constants for this important flame–chemistry reaction have been measured at 787 K by Shi and Marshall (1991), and we have assumed a temperature dependence based on other typical termolecular reactions (see also Schofield and Steinberg 1992). Ionospheric reactions such as R649 ($SO^+ + Na \rightarrow Na^+ + SO$), R540 ($Na + h\nu \rightarrow Na^+ + e^-$), and R641 ($S_2^+ + Na \rightarrow Na^+ + S_2$) account for $\sim$28% of the total Na destruction rate. Other three-body reactions that produce sodium molecules (e.g., reaction R279, $S_2 + Na + M \rightarrow NaS_2 + M$) account for $<$2% of the Na destruction rate, and reactions that recycle NaCl (e.g., reaction R455, $S_2Cl + Na \rightarrow NaCl + S_2$) account for $<$1% of the total Na destruction rate (see Table II).

Sodium chloride and atomic Na are the only vapor-phase sodium species that are abundant enough in our moderate-density

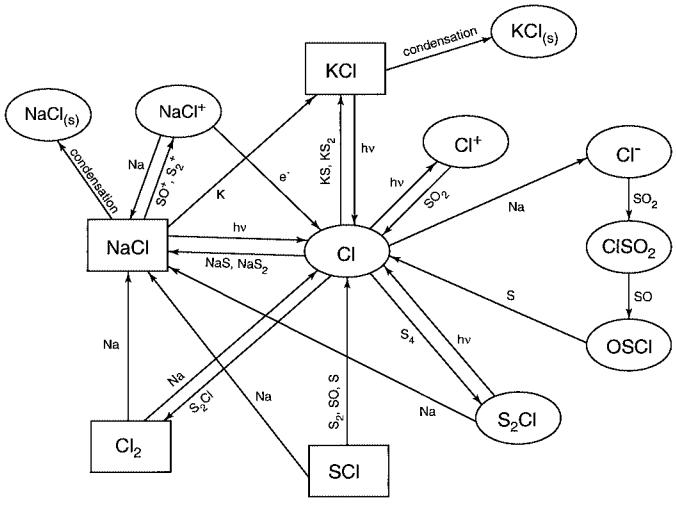

FIG. 3. A schematic diagram illustrating the important reaction pathways for chlorine species in our standard moderate-density model. The symbols are described in Fig. 2.

TABLE II
Important Photochemical Production and Loss Mechanisms

Species		Reaction	Column-integrated rate (cm^{-2} s^{-1})	% of total rate
NaCl	Production	R372: $Cl + NaS \rightarrow NaCl + S$	4.42×10^7	28.0%
		R373: $Cl + NaS_2 \rightarrow NaCl + S_2$	4.18×10^7	26.5%
		R377: $Cl + NaSO_2 \rightarrow NaCl + SO_2$	1.86×10^7	11.8%
		R455: $S_2Cl + Na \rightarrow NaCl + S_2$	1.81×10^7	11.5%
		R445: $SCl + Na \rightarrow NaCl + S$	1.53×10^7	9.7%
		R685: $NaCl^+ + Na \rightarrow Na^+ + NaCl$	1.15×10^7	7.3%
		R376: $Cl + NaOS \rightarrow NaCl + SO$	4.59×10^6	2.9%
		all other reactions	3.52×10^6	2.2%
	Loss	R50: $NaCl + h\nu \rightarrow Na + Cl$	3.49×10^{11}	51.9%
		R506: $NaCl + dust \rightarrow NaCl_{(con)}$	3.22×10^{11}	48.0%
		all other reactions	7.46×10^8	0.1%
Na	Production	R50: $NaCl + h\nu \rightarrow Na + Cl$	3.49×10^{11}	99.6%
		R484: $NaCl + K \rightarrow KCl + Na$	6.98×10^8	0.2%
		R338: $SO + NaS \rightarrow S_2O + Na$	4.41×10^8	0.1%
		R251: $S + NaS \rightarrow Na + S_2$	2.99×10^8	0.1%
		all other reactions	1.05×10^8	trace
	Loss	R342: $SO_2 + Na + M \rightarrow NaSO_2 + M$	2.79×10^9	68.8%
		R649: $SO^+ + Na \rightarrow Na^+ + SO$	5.42×10^8	13.4%
		R540: $Na + h\nu \rightarrow Na^+ + e^-$	4.21×10^8	10.4%
		R641: $S_2^+ + Na \rightarrow Na^+ + S_2$	1.21×10^8	3.0%
		R279: $S_2 + Na + M \rightarrow NaS_2 + M$	3.97×10^7	1.0%
		R471: $Na + NaSO_2 \rightarrow Na_2 + SO_2$	2.72×10^7	0.7%
		R336: $SO + Na + M \rightarrow NaOS + M$	2.11×10^7	0.5%
		R637: $S^+ + Na \rightarrow Na^+ + S$	1.82×10^7	0.4%
		R455: $S_2Cl + Na \rightarrow NaCl + S_2$	1.81×10^7	0.4%
		R445: $SCl + Na \rightarrow NaCl + S$	1.53×10^7	0.4%
		all other reactions	4.50×10^7	1.1%
$NaSO_2$	Production	R342: $SO_2 + Na + M \rightarrow NaSO_2 + M$	2.79×10^9	100.0%
	Loss	R280: $S_2 + NaSO_2 \rightarrow NaS_2 + SO_2$	6.10×10^8	54.9%
		R339: $SO + NaSO_2 \rightarrow NaOS + SO_2$	3.58×10^8	32.2%
		R255: $S + NaSO_2 \rightarrow NaS + SO_2$	9.12×10^7	8.2%
		R471: $Na + NaSO_2 \rightarrow Na_2 + SO_2$	2.72×10^7	2.4%
		R377: $Cl + NaSO_2 \rightarrow NaCl + SO_2$	1.86×10^7	1.7%
		all other reactions	6.98×10^6	0.6%
NaOS	Production	R339: $SO + NaSO_2 \rightarrow NaOS + SO_2$	3.58×10^8	94.4%
		R336: $SO + Na + M \rightarrow NaOS + M$	2.11×10^7	5.6%
	Loss	R254: $S + NaOS \rightarrow NaS + SO$	2.77×10^8	98.0%
		R376: $Cl + NaOS \rightarrow NaCl + SO$	4.59×10^6	1.6%
		R108: $O + NaOS \rightarrow Na + SO_2$	6.02×10^5	0.2%
		all other reactions	4.01×10^5	0.1%
NaS_2	Production	R280: $S_2 + NaSO_2 \rightarrow NaS_2 + SO_2$	6.10×10^8	93.9%
		R279: $S_2 + Na + M \rightarrow NaS_2 + M$	3.97×10^7	6.1%
	Loss	R252: $S + NaS_2 \rightarrow NaS + S_2$	4.13×10^8	86.1%
		R373: $Cl + NaS_2 \rightarrow NaCl + S_2$	4.18×10^7	8.7%
		R48: $NaS_2 + h\nu \rightarrow Na + S_2$	2.41×10^7	5.0%
		all other reactions	8.33×10^5	0.2%
KCl	Production	R484: $NaCl + K \rightarrow KCl + Na$	6.98×10^8	95.3%
		R386: $Cl + KS \rightarrow KCl + S$	2.36×10^7	3.2%
		R387: $Cl + KS_2 \rightarrow KCl + S_2$	6.19×10^6	0.8%
		R389: $Cl + KSO_2 \rightarrow KCl + SO_2$	2.68×10^6	0.4%
		all other reactions	1.94×10^6	0.3%
	Loss	R54: $KCl + h\nu \rightarrow K + Cl$	4.91×10^{10}	66.2%
		R514: $KCl + dust \rightarrow KCl_{(con)}$	2.51×10^{10}	33.8%
		all other reactions	4.13×10^6	trace

TABLE II—*Continued*

Species		Reaction	Column-integrated rate (cm^{-2} s^{-1})	% of total rate
K	Production	R54: $KCl + h\nu \rightarrow K + Cl$	4.91×10^{10}	99.5%
		R262: $S + KS \rightarrow K + S_2$	2.20×10^{8}	0.4%
		all other reactions	6.21×10^{6}	trace
	Loss	R484: $NaCl + K \rightarrow KCl + Na$	6.98×10^{8}	65.5%
		R344: $SO_2 + K + M \rightarrow KSO_2 + M$	2.43×10^{8}	22.9%
		R541: $K + h\nu \rightarrow K^+ + e^-$	5.71×10^{7}	5.4%
		R651: $SO^+ + K \rightarrow K^+ + SO$	5.06×10^{7}	4.8%
		R644: $S_2^+ + K \rightarrow K^+ + S_2$	8.98×10^{6}	0.8%
		all other reactions	6.68×10^{6}	0.6%
Cl	Production	R50: $NaCl + h\nu \rightarrow Na + Cl$	3.49×10^{11}	87.6%
		R54: $KCl + h\nu \rightarrow K + Cl$	4.91×10^{10}	12.3%
		all other reactions	8.00×10^{7}	trace
	Loss	R372: $Cl + NaS \rightarrow NaCl + S$	4.42×10^{7}	25.5%
		R373: $Cl + NaS_2 \rightarrow NaCl + S_2$	4.18×10^{7}	24.1%
		R386: $Cl + KS \rightarrow KCl + S$	2.36×10^{7}	13.6%
		R307: $S_4 + Cl \rightarrow S_2 + S_2Cl$	2.19×10^{7}	12.6%
		R377: $Cl + NaSO_2 \rightarrow NaCl + SO_2$	1.86×10^{7}	10.7%
		R387: $Cl + KS_2 \rightarrow KCl + S_2$	6.19×10^{6}	3.6%
		R536: $Cl + h\nu \rightarrow Cl^+ + e^-$	5.43×10^{6}	3.1%
		R376: $Cl + NaOS \rightarrow NaCl + SO$	4.59×10^{6}	2.6%
		R725: $Na + Cl \rightarrow Na^+ + Cl^-$	3.04×10^{6}	1.8%
		R389: $Cl + KSO_2 \rightarrow KCl + SO_2$	2.68×10^{6}	1.5%
		all other reactions	1.42×10^{6}	0.8%

model to be potentially observable with current technologies. However, the photochemical production of molecules such as $NaSO_2$, NaS_2, Na_2, and NaOS becomes more important as the total atmospheric density increases because of the importance of three-body reactions in the production mechanisms. The dominant sodium-sulfur species, $NaSO_2$, is synthesized by the three-body addition of Na and SO_2 (reaction R342). Following the flame chemistry study of Schofield and Steinberg (1992), we have assumed that $NaSO_2$ is lost by reactions such as R280 ($S_2 + NaSO_2 \rightarrow NaS_2 + SO_2$; ~55% of total column destruction rate), R339 ($SO + NaSO_2 \rightarrow NaOS + SO_2$; ~32% of total destruction rate), R255 ($S + NaSO_2 \rightarrow NaS + SO_2$; ~8% of total destruction rate), R471 ($Na + NaSO_2 \rightarrow Na_2 + NaSO_2$; ~2% of total destruction rate), and R377 ($Cl + NaSO_2 \rightarrow NaCl + SO_2$; ~2% of total destruction rate; see Table II). Thus, $NaSO_2$ destruction is often the dominant pathway for the production of many other sodium molecules. Other important production pathways are three-body recombination reactions such as R336 ($SO + Na + M \rightarrow NaOS + M$) and R279 ($S_2 + Na + M \rightarrow NaS_2 + M$).

3.2. Potassium Photochemistry

Potassium photochemistry is largely initiated by the photolysis of volcanic KCl and by the chemical destruction of K. As with NaCl, the photolysis rate of KCl greatly exceeds its photochemical production, and KCl will be rapidly lost from Io's atmosphere if volcanic sources (or sputtering) are not available for replenishment.

Atomic K, like atomic Na, is relatively stable photochemically (see Table II). It is produced predominantly from KCl photolysis and from volcanic sources, with a lesser contribution from reaction R262 ($S + KS \rightarrow K + S_2$). The dominant atomic K destruction mechanisms in our model are reaction R484 ($NaCl + K \rightarrow KCl + Na$) and R344 ($K + SO_2 + M \rightarrow KSO_2 + M$). The photochemistry of potassium species has been less well studied than that of sodium species, and our results for the abundances of the potassium compounds are therefore more uncertain. However, KCl and K should remain the dominant potassium-bearing species regardless of the adopted rate coefficients.

3.3. Chlorine Photochemistry

Preliminary estimates of the important pathways for chlorine photochemistry were discussed by Küppers and Schneider (2000). In our moderate-density model, chlorine photochemistry is initiated by the destruction of volcanic NaCl and KCl. As discussed above, recycling mechanisms for NaCl and KCl are inefficient—these species would disappear from the atmosphere if volcanic sources were not available for their replenishment.

Photolysis of NaCl (R50) is the largest photochemical source of atomic chlorine (~87% of the total column production rate), followed by KCl photolysis (~13% of total production; see

Table II). Atomic Cl is lost by reaction with NaS and NaS_2 (reactions R372 and R373; ~26% and 24%, respectively, of the total column destruction rate), by reaction with volcanic KS (reaction R386; ~14% of the total destruction rate), by reaction with S_4 (reaction R307; ~13% of total destruction rate), and by other reactions with sodium–sulfur and potassium–sulfur species such as $NaSO_2$, KS_2, and KSO_2 (e.g., R377, R387, R389; see Fig. 3 and Table II). The main products in most of these reactions are NaCl and KCl. As with atomic Na and K, the photochemical production rate of atomic Cl greatly exceeds its photochemical loss rate.

Chlorine oxides are not very important in our photochemical model. The dominant chlorine oxide, ClO, is produced largely from reaction R93 ($O + ClSO_2 \rightarrow SO_2 + ClO$) through an unusual (and speculative) reaction scheme derived from flame-chemistry studies:

$$\begin{aligned} Na + Cl &\rightarrow Na^+ + Cl^- && \text{R725}\\ Cl^- + SO_2 &\rightarrow ClSO_2 + e^- && \text{R735}\\ O + ClSO_2 &\rightarrow SO_2 + ClO && \text{R93}\\ \hline \text{Net: } Cl + O + Na &\rightarrow ClO + Na^+ + +e^-. && (1) \end{aligned}$$

In a more traditional reaction scheme, R725 and R735 above are replaced by R340 ($SO_2 + Cl + M \rightarrow ClSO_2 + M$). ClO is readily lost by reaction with S, SO, S_2, and Na (e.g., reactions R229, R329, R410, and R276).

Sulfur chlorides are somewhat more important than chlorine oxides in our model. The dominant sulfur chloride, S_2Cl, is produced from the reaction of Cl and S_4 through the scheme

$$\begin{aligned} 2S_2 &\overset{M}{\rightarrow} S_4 && \text{R268}\\ S_4 + Cl &\rightarrow S_2 + S_2Cl && \text{R307}\\ \hline \text{Net: } S_2 + Cl &\rightarrow S_2Cl. && (2) \end{aligned}$$

S_2Cl is lost predominantly by reaction with atomic Na (reaction R455, $S_2Cl + Na \rightarrow NaCl + S_2$) and by photolysis (e.g., reaction R36, $S_2Cl + h\nu \rightarrow S_2 + Cl$). All of the production and loss mechanisms for S_2Cl are speculative.

Molecular chlorine, Cl_2, is produced by reaction R360 ($Cl + OSCl \rightarrow SO + Cl_2$; ~72% of the total column production rate), and by reaction R358 ($Cl + S_2Cl \rightarrow S_2 + Cl_2$; ~27% of the total production rate). Molecular chlorine is lost by reaction R394 ($Cl_2 + Na \rightarrow NaCl + Cl$; ~97% of the total column loss rate), and by reaction R395 ($Cl_2 + K \rightarrow KCl + Cl$; ~3% of total loss rate).

Sulfuryl chloride, SO_2Cl_2, is not a major gas in the thermochemical equilibrium models of Pele-type volcanic eruptions on Io (see Fegley and Zolotov 2000 and Table I), and we predict that SO_2Cl_2 will not be produced readily by gas-phase photochemical reactions in Io's low-density atmosphere. The dominant production mechanism in our moderate-density model is R462 ($2\ ClSO_2 \rightarrow SO_2Cl_2 + SO_2$). The dominant loss processes for SO_2Cl_2 are reaction R466 ($SO_2Cl_2 + Na \rightarrow NaCl + ClSO_2$; ~84% of total column destruction rate) and reaction R363 ($Cl + SO_2Cl_2 \rightarrow ClSO_2 + Cl_2$; ~16% of destruction rate). However, as will be discussed below (Section 7), heterogeneous reactions at Io's surface might enhance the abundance of condensed SO_2Cl_2.

4. SENSITIVITY STUDIES

The derived species concentrations presented in Fig. 1 and the inferred major production and loss pathways described in the previous section depend on several assumptions of our modeling. We now examine the sensitivity of our results to changes in the atmospheric density, in the eddy diffusion coefficients, in the condensation efficiency, in certain key reaction rates, and in the assumed elemental composition of the volcanic gases.

4.1. Sensitivity to Atmospheric Density

Our high-density model has a surface density (and a total atmospheric column density) that is ~8.5 times that of the moderate-density model, and our low-density model has a surface density that is ~5.5 times smaller than the moderate-density model. One might then expect the steady-state column densities of the volcanic species to be uniformly larger (or smaller) in the high-density (or low-density) model than in the moderate-density model. While this result is generally true, the complicated and nonlinear response of photochemistry keeps the column-density increase from being linear. Figure 4 illustrates how the concentrations of the major alkali and chlorine species are altered when the atmospheric density is increased. Because other properties, such as the eddy diffusion coefficient, the dust concentration profile, and the relative abundances of the volcanic gases at the lower boundary, are kept the same in this model as in our moderate-density model, the results in Fig. 4 can be directly compared with those in Fig. 1.

When the atmospheric density is increased, both atomic and molecular species tend to have greater overall concentrations, especially at low altitudes. Molecular concentrations, however, tend to increase more dramatically than atomic concentrations. Part of this effect is due to the increased efficiency of three-body reactions when the atmospheric density is increased. For instance, sulfur–alkali and sulfur–chlorine species such as $NaSO_2$, NaS_2, and S_2Cl that depend on termolecular reactions such as R342 ($Na + SO_2 + M \rightarrow NaSO_2 + M$) or R268 ($2\ S_2 + M \rightarrow S_4 + M$) for their synthesis exhibit dramatically enhanced concentrations in the lower atmosphere because all three components required for their production have been increased. Recycling reactions also tend to become more efficient as molecular abundances increase. For example, the rates of reactions such as R455 ($S_2Cl + Na \rightarrow NaCl + S_2$) that recycle NaCl are many orders of magnitude larger when the atmospheric density is increased from the low- to moderate-density case or from the moderate- to high-density case. Therefore, even though NaCl loss rates have increased, the total column density of NaCl

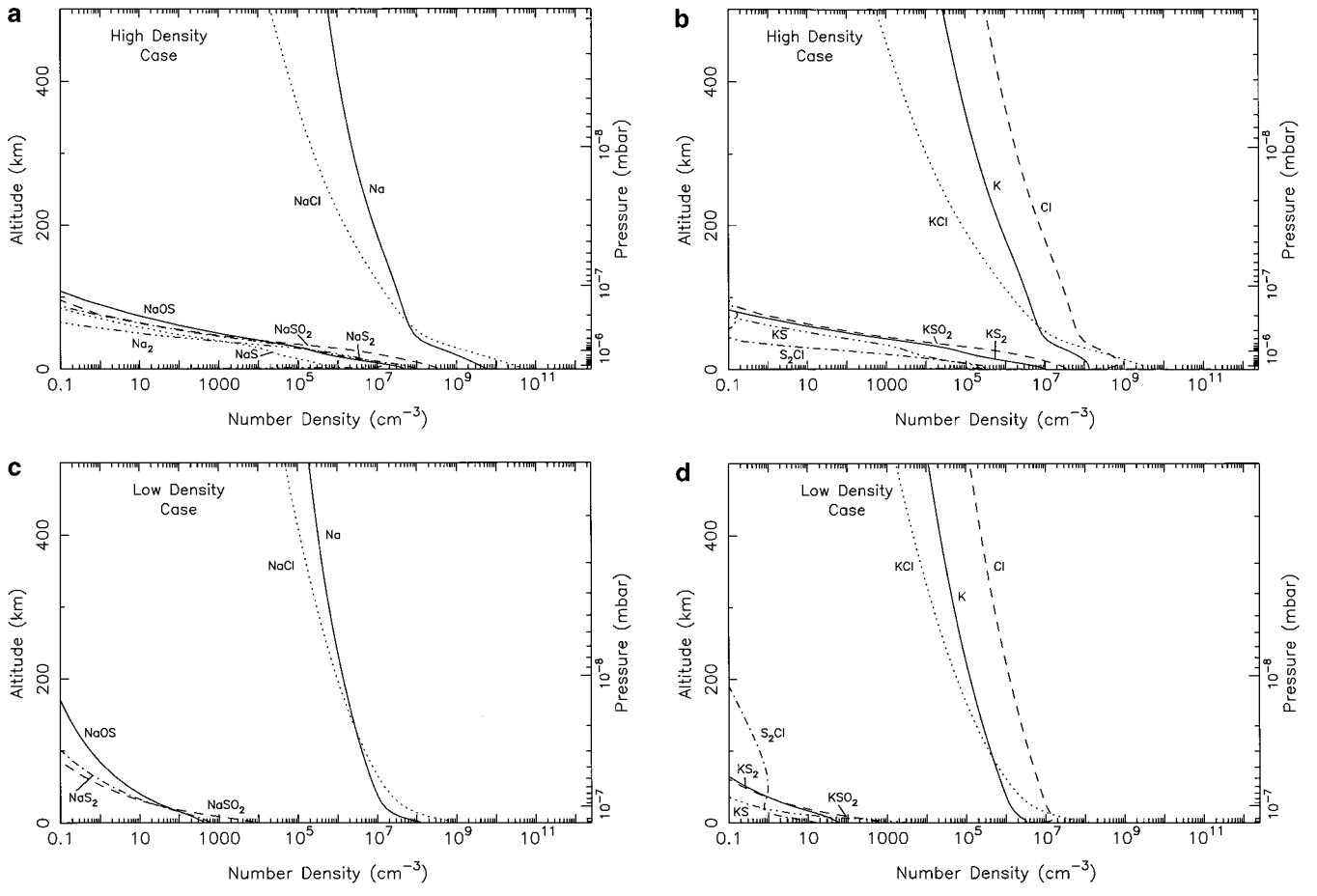

FIG. 4. The concentrations of several important atmospheric constituents in our high-density model (e.g., 18 nanobar surface pressure, SO_2 column density 7.4×10^{17} cm^{-2}, $K_E = 10^9$ cm^2 s^{-1}) as a function of altitude and pressure: (a) sodium species, and (b) potassium and chlorine species, and in our low-density model (e.g., 0.37 nanobar surface pressure, SO_2 column density 1.5×10^{16} cm^{-2}, $K_E = 10^9$ cm^2 s^{-1}): (c) sodium species, and (d) potassium and chlorine species.

increases to a larger degree than the total atmospheric density increase.

Table I, which shows how the column-integrated mixing ratios change when the atmospheric density changes, further demonstrates the increased importance of alkali and chlorine molecules as opposed to atoms in the high-density model (in terms of total column abundance). Three-body reactions such as R342, R343, and R455 allow the loss rates for atomic species such as Na and K in the high-density case to approach their production rates—a situation much different from the moderate- and low-density atmospheric models (see Section 3). The relative importance of these atoms is therefore reduced in the high-density model. Two-body reactions, whose rates generally increase when molecular concentrations increase, also contribute to the trend toward atomic species becoming relatively less important at higher atmospheric densities.

On the other hand, lower density atmospheres are more likely to be hotter and to contain molecular constituents at high altitudes. Because of the differences in the temperature profiles of the three models (see Paper 1), the scale heights of the diffusion-dominated species in the upper atmosphere are larger for the lower density models. Therefore, molecular species such as NaCl and KCl tend to become more abundant at high altitudes in the lower density models than in the higher density models. Heavier species are more sensitive to this effect.

4.2. Sensitivity to Eddy Diffusion Coefficient

Figure 5 illustrates how the concentrations of important alkali and chlorine species change when the eddy diffusion coefficient is reduced from $K_E = 10^9$ cm^2 s^{-1} (SO_2 homopause at ~34 km altitude) to $K_E = 10^8$ cm^2 s^{-1} (SO_2 homopause at ~16 km altitude). For species that are produced predominantly from volcanic rather than photochemical sources (e.g., NaCl and KCl), the reduction in K_E inhibits the gases from being mixed to as high altitudes, causing a reduction in the total column abundances of the the parent volcanic gases when K_E is reduced. For instance, when the eddy diffusion coefficient is reduced to 10^8 cm^2 s^{-1}, the column densities of both NaCl and KCl are a factor of 1.43 times smaller than what they were in the $K_E = 10^9$ cm^2 s^{-1} model (cf. Figs. 1 and 5); note that changes in photochemical loss processes and in diffusion have affected this

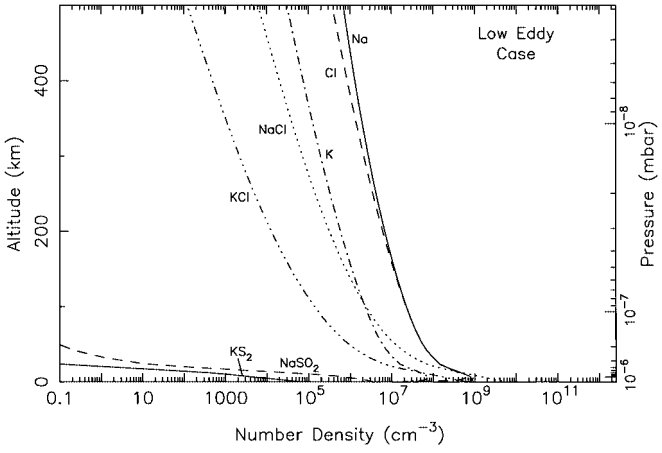

FIG. 5. The concentrations of several important alkali and chlorine species in our moderate-density low-eddy diffusion model (e.g., for an assumed altitude-independent eddy diffusion coefficient of $K_E = 10^8$ cm^2 s^{-1}).

value). For species such as Na, K, Cl, KSO_2, and $NaSO_2$ that are produced predominantly from photochemical sources (volcanic influx is less important for atomic Na, K, and Cl than photochemical production), the downward flux at the lower boundary is smaller when the eddy diffusion coefficient is reduced; the lifetime of these species against diffusion to the surface then increases when K_E is decreased, which tends to result in larger column densities for photochemically produced species. As a general rule, species that are highly reactive or that have complicated nonlinear production and loss mechanisms (such as the heavy sulfur–alkali and sulfur–halogen molecules) show pronounced changes when K_E is reduced.

4.3. Sensitivity to Condensation Efficiency

As mentioned in Section 3, the photochemical model results for the alkali and chlorine species are very sensitive to assumptions about the efficiency of NaCl and KCl condensation. To truly determine the degree of partitioning of NaCl and KCl between the gas and solid phases, we would need to accurately model the complex problem of condensation within a rapidly expanding volcanic plume. Such modeling is beyond the scope of this work, and we instead use a much simpler technique to estimate the condensation rate of supersaturated vapor about preexisting atmospheric aerosols (see the Appendix). For aerosol particles in the free-molecular flow regime, which is relevant throughout Io's atmosphere, the condensation rate using this simplified technique varies linearly with the particle concentration and with the square of the particle radius. The efficiency of condensation can thus be altered by varying the particle concentration or radius.

Assumptions about the condensation efficiency in the model can dramatically affect the resulting partitioning of sodium, potassium, and chlorine among the different species. For example, in our standard moderate-density model, roughly 19% of the sodium is tied up in gas-phase atomic Na, 76% is tied up in NaCl vapor, and 4.7% is tied up in condensed NaCl. When condensation is assumed to be 10 times more efficient than in our standard moderate-density model, these fractions change to 13% of the sodium tied up in atomic Na, 53% tied up in NaCl vapor, and 33% tied up in condensed NaCl. Without condensation, ~20% of the sodium is tied up in atomic Na and ~80% in NaCl vapor. Because less NaCl and KCl vapor is available when condensation is more efficient, the photolysis source providing atomic Na, K, and Cl is reduced, and the subsequent production of most sodium, potassium, and chlorine species is inhibited. Alkali and chlorine molecules therefore tend to be less abundant when condensation is effecient.

4.4. Sensitivity to Key Reaction Rates

Many of the rate coefficients for the reactions listed in the Appendix have not been investigated experimentally or theoretically. Because of interest in metal chemistry in the Earth's atmosphere, alkali–oxygen reactions have been well studied, but information on reactions involving alkali–sulfur interactions is particularly inadequate (with the exception of a few flame-chemistry studies; see Schofield and Steinberg 1992 and references therein). We now examine the sensitivity of our results to the rate coefficients adopted for certain important but ill-constrained reactions.

Sodium chloride photolysis initiates much of the alkali and chlorine photochemistry in our model (see Figs. 2 and 3). Room temperature cross sections for NaCl have been presented by Silver *et al.* (1986). Although the error bars on these measurements are not large, the temperature dependence of the cross sections is unknown, and we estimate that for our situation, the cross sections could be uncertain by a factor of ~1.5. Table III demonstrates how the concentrations of important alkali and chlorine species change relative to our standard moderate-density model when the cross sections σ_{50} for NaCl photolysis are varied by a factor of 1.5 at all wavelengths. When the cross section is increased, NaCl photolysis is more effective (such that the NaCl abundance decreases), and the production rates of most other alkali and chlorine species increase. Note that KCl is an exception to this trend. When NaCl is less abundant, production (recycling) of KCl through reaction R484 ($NaCl + K \rightarrow KCl + Na$) is less effective, and the KCl abundance decreases. Although virtually all alkali and chlorine species are affected by changes in σ_{50}, the effects are not large for reasonable uncertainties in the NaCl cross sections.

The most abundant alkali–sulfur molecule in our model is $NaSO_2$. As discussed in Section 4, $NaSO_2$ is produced mainly by reaction R342 ($SO_2 + Na + M \rightarrow NaSO_2 + M$). This important three-body reaction also influences the abundance of species such as NaS_2, NaS, and NaOS. Although both the low- and high-pressure limiting rate coefficients for reaction R342 have been measured at 787 K in the flash-photolysis experiments of Shi and Marshall (1991), the temperature dependence of the rate coefficients is uncertain. We have assumed that the reaction proceeds at its low-pressure limit in Io's tenuous atmosphere and that the reaction becomes more efficient at low

TABLE III
Change Relative to Standard Moderate-Density Model

Constituent	$\sigma_{50} \times 1.5$	$\sigma_{50} \div 1.5$	$k_{338} \times 6$	$k_{338} \div 6$	$k_{455} \div 100$	$k_{342} = 2.55 \times 10^{-29}$
Cl	+28%	−23%	+0.1%	+0.0%	+0.0%	+0.1%
Cl_2	+24%	−24%	+0.0%	+0.0%	+7.1%	+0.0%
SCl	+12%	−13%	+0.0%	+0.0%	+0.0%	+0.0%
S_2Cl	+28%	−23%	+0.0%	+0.0%	+500%	+0.0%
$ClSO_2$	+28%	−27%	+0.0%	+0.0%	+0.0%	+0.0%
SO_2Cl_2	+45%	−39%	+0.0%	+0.0%	+0.0%	+0.0%
Na	+13%	−12%	+0.0%	+0.0%	+0.0%	+0.0%
Na_2	+13%	−8.8%	+0.0%	+0.0%	+0.0%	−98%
NaS	+0.3%	+0.0%	−70%	+86%	+0.0%	−94%
NaS_2	+1.8%	−1.2%	+0.0%	+0.0%	+0.0%	−92%
Na_2S	+2.5%	−1.5%	−76%	+134%	+0.0%	−92%
NaOS	+3.8%	−2.7%	+0.0%	+0.0%	+0.0%	−93%
$NaSO_2$	+4.2%	−2.8%	+0.0%	+0.0%	+0.0%	−98%
NaCl	−3.0%	+2.7%	+0.0%	+0.0%	+0.0%	+0.0%
K	+23%	−20%	+0.0%	+0.0%	+0.0%	+0.0%
KS	+0.8%	−0.6%	+0.0%	+0.0%	+0.0%	+0.0%
KS_2	+15%	−11%	+0.0%	+0.0%	+0.0%	+0.0%
KSO_2	+18%	−13%	+0.0%	+0.0%	+0.0%	+0.0%
KCl	−3.3%	+2.8%	+0.0%	+0.0%	+0.0%	+0.0%

Note. Numbers in this table represent the change in the column-integrated mixing ratios (i.e., the column denisty of the consituent divided by the SO_2 column density). Changes of less than 1% are not significant.

temperatures (as is typical for termolecular reactions). If, however, we were to adopt a temperature-independent low-pressure limiting rate coefficient of $k_{342} = 2.55 \times 10^{-29}$ cm^6 s^{-1} (Shi and Marshall's value at 787 K), we would find that the abundances of the sodium-bearing molecules Na_2, Na_2S, NaS, NaS_2, NaOS, $NaSO_2$ are reduced by factors of 12–50 compared with our standard moderate-density model (see Table III). Potassium- and chlorine-bearing species are unaffected by the change in k_{342}.

We have also examined the effects of a factor of 6 change in the adopted rate coefficient for reaction R338 ($SO + NaS \rightarrow S_2O + Na$) and the effects of a factor of 10 or 100 reduction in the rate coefficient for reaction R455 ($S_2Cl + Na \rightarrow NaCl + S_2$)—speculative reactions that involve sodium–sulfur interactions. We find that k_{338} mainly affects the NaS and Na_2S abundances and has little effect on other molecules. Similarly, k_{455} mainly affects S_2Cl, and to a lesser extent Cl_2, and has little effect on other atmospheric constituents.

In all, the results seem to be less sensitive to changes in uncertain reaction rates than they are to changes in other uncertain parameters such as the eddy diffusion coefficient, the total atmospheric density, or the efficiency of condensation. Photolysis of NaCl and KCl control the abundances of the other alkali and halogen species, and as long as the volcanoes are active, NaCl, Na, Cl, KCl, and K will be the most abundant alkali and chlorine species in our model regardless of the assumed rate coefficients. On the other hand, reactions such as R342 can affect the relative importance of alkali-sulfur molecules, and further laboratory experiments that constrain the temperature dependence of the reaction rate would be useful for photochemical modeling of Io's atmosphere.

4.5. Sensitivity to the Na/Cl Ratio

Our standard moderate-density model has specific assumptions about the relative abundances of the different elements within the exsolved volcanic vapor—we have adopted elemental ratios of 1.521-1.0-0.05-0.005-0.05 for O-S-Na-K-Cl for our standard model based on observations of SO_2, SO, S, and S_2 in the Pele plume and of ions in the Io torus (see Zolotov and Fegley 2000 and Paper 1). However, the relative abundances of the elements in Io's atmosphere are uncertain, and different assumptions could result in different molecules or atoms becoming important constituents in our model. For example, our standard model has a Na/Cl ratio of 1, causing NaCl to be the dominant reservoir for both sodium and chlorine. If either sodium or chlorine were to dominate over the other, the excess of either element could cause some interesting photochemical differences. We therefore examine the sensitivity of our results to assumptions about the elemental ratios of the volcanic vapor. In particular, we examine the sensitivity of the results to changes in the Na/Cl ratio.

Küppers and Schneider (2000) have determined that the total chlorine density within the Io torus lies between 1.5 and 5.5% of all ions; their preferred value is 2% (note, however, that this percentage has recently been revised upward because of the detection of Cl^{++} in the torus; Schneider *et al*. 2000). In our standard photochemical model, we have assumed that the torus population reflects the vapor population on Io, and we have adopted a 2% elemental chlorine abundance. We now consider an extended range of possible chlorine abundances. For our chlorine-enriched model, we have assumed that Cl makes up 5.5% of all

the elements (upper limit of Küppers and Schneider 2000 for chlorine in the torus). The abundances of the other elements relative to sulfur are kept the same as in our standard model, such that O/S = 1.521, Na/S = 0.05, and K/S = 0.005. After some algebraic manipulation, one can determine that our chlorine-enriched case has a Cl/S ratio of 0.15 and a Cl/Na ratio of 3.

For our sodium-enriched model, we assume that chlorine ions make up 1.5% of the ions in the torus (lower limit from Küppers and Schneider 2000) and that Na^+ makes up 4.5% of the torus ions (upper limit from Bagenal and Sullivan 1981). As in our standard model, potassium is assumed to be one-tenth as abundant as sodium, and the O/S ratio is kept at 1.521. Our elemental ratios for this sodium-enriched model thus become O-S-Na-K-Cl = 1.521-1.0-0.12-0.012-0.04, and the model has a Na/Cl ratio of 3. These elemental ratios are plugged back into the thermochemical equilibrium code (again assuming a magma temperature of 1440 K and a vent pressure of 6.9×10^{-6} bars) to derive new mixing ratios for the volcanic species; the derived mixing ratios are in turn used as boundary conditions for the new sodium-enriched or chlorine-enriched photochemical models.

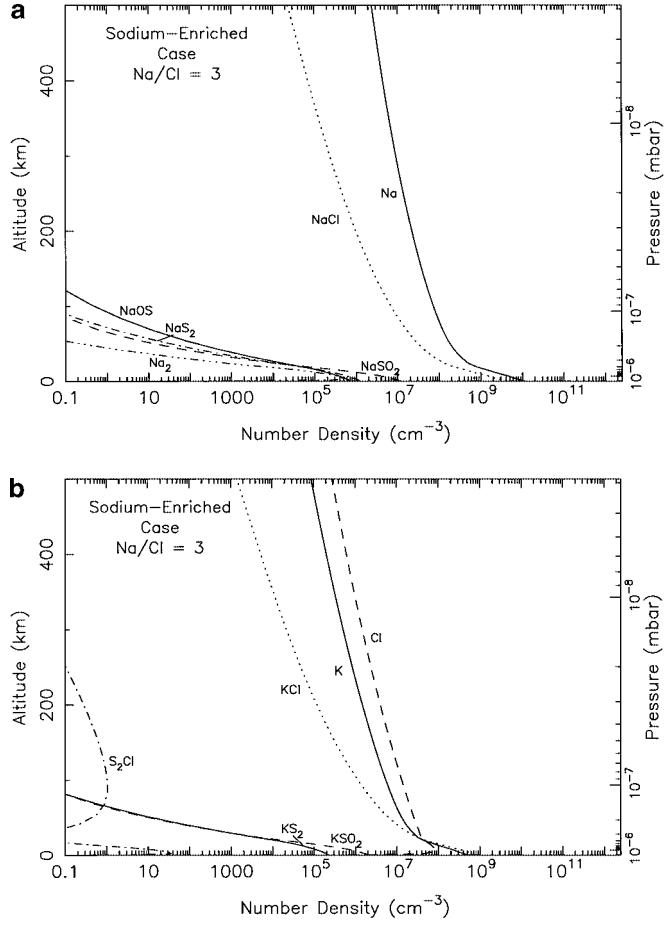

FIG. 6. The concentrations of several important atmospheric constituents in our sodium-enriched model as a function of altitude and pressure: (a) sodium species, and (b) potassium and chlorine species.

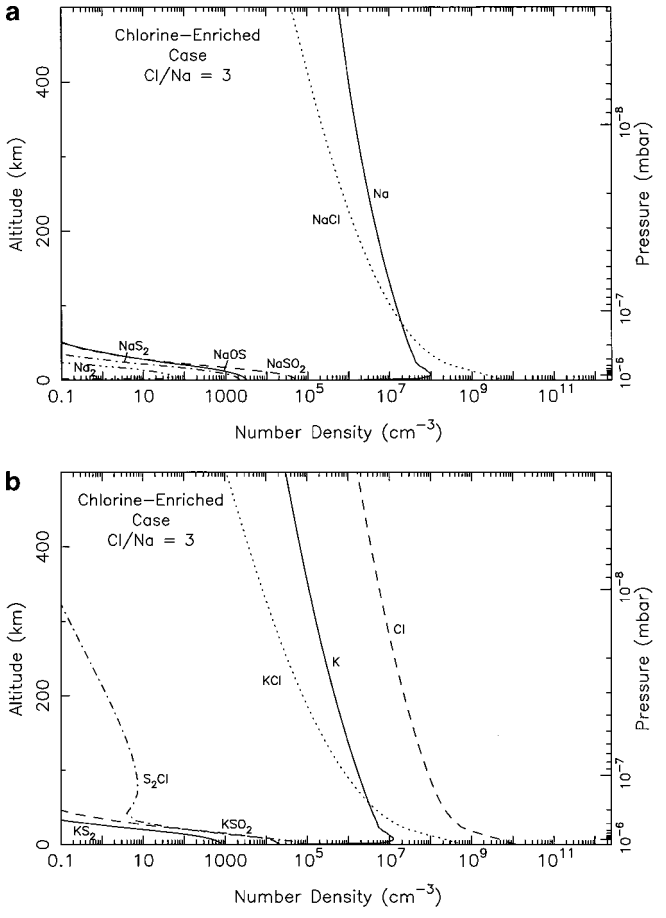

FIG. 7. The concentrations of several important atmospheric constituents in our chlorine-enriched model as a function of altitude and pressure: (a) sodium species, and (b) potassium and chlorine species.

Figures 6 and 7 show the concentrations of the important alkali and chlorine species in our sodium-enriched and chlorine-enriched models. The column-integrated mixing ratios of the various alkali and chlorine species are shown in Table IV to aid in comparison with our standard model (cf. Table I). Note from both the figures and the tables that the same five species (NaCl, Na, Cl, KCl, K) dominate the gas-phase abundances in all models; however, the relative abundances of these five species change in each model. In our standard model, NaCl dominates. In the sodium-enriched model, the excess sodium exists largely as atomic Na. In the chlorine-enriched model, the excess chlorine exists largely as atomic Cl. The concentrations of sulfur-chlorine and sulfur-sodium molecules also change dramatically between the three models, but the column densities of these molecules never exceed 10^{13} cm^{-2}; i.e., these molecules are never major atmospheric constituents. The NaCl and KCl abundances are relatively insensitive to changes in the Na/Cl ratio as compared with Na, K, Cl, and the sodium–sulfur or chlorine–sulfur molecules, whose abundances change dramatically between the three models.

TABLE IV
Abundance Relative to SO_2

Constituent	Sodium-enriched case		Chlorine-enriched case	
	Initial	Final	Initial	Final
Cl	7.68×10^{-6}	5.71×10^{-3}	1.29×10^{-1}	1.43×10^{-1}
Cl_2	2.07×10^{-13}	2.16×10^{-11}	5.78×10^{-5}	1.17×10^{-5}
ClO	3.24×10^{-13}	2.15×10^{-10}	5.43×10^{-9}	2.09×10^{-9}
ClOO	—	2.76×10^{-16}	—	6.40×10^{-15}
OClO	—	3.92×10^{-32}	—	2.98×10^{-30}
Cl_2O	7.96×10^{-25}	2.80×10^{-24}	2.22×10^{-16}	2.85×10^{-17}
Cl_2O_2	—	8.08×10^{-30}	—	1.64×10^{-26}
SCl	4.01×10^{-10}	1.14×10^{-9}	6.70×10^{-6}	9.67×10^{-7}
SCl_2	2.36×10^{-16}	4.19×10^{-17}	6.53×10^{-8}	1.73×10^{-8}
S_2Cl	3.54×10^{-11}	4.38×10^{-10}	5.86×10^{-7}	5.46×10^{-7}
S_2Cl_2	2.01×10^{-20}	2.56×10^{-21}	5.53×10^{-12}	1.27×10^{-12}
OSCl	—	3.19×10^{-9}	—	1.24×10^{-8}
$ClSO_2$	—	2.39×10^{-8}	—	8.65×10^{-8}
$SOCl_2$	7.46×10^{-18}	—	2.06×10^{-9}	—
SO_2Cl_2	1.20×10^{-24}	9.67×10^{-14}	3.30×10^{-16}	2.54×10^{-12}
Na	1.20×10^{-1}	1.31×10^{-1}	1.12×10^{-5}	6.63×10^{-3}
Na_2	2.22×10^{-9}	5.15×10^{-6}	1.90×10^{-17}	5.70×10^{-10}
NaO	5.78×10^{-8}	1.41×10^{-8}	5.38×10^{-12}	1.22×10^{-11}
NaO_2	—	7.51×10^{-12}	—	1.70×10^{-14}
NaO_3	—	8.45×10^{-19}	—	7.76×10^{-22}
Na_2O	2.12×10^{-12}	1.42×10^{-12}	1.82×10^{-20}	1.45×10^{-20}
NaS	—	4.04×10^{-7}	—	3.83×10^{-10}
NaS_2	—	1.28×10^{-5}	—	2.41×10^{-8}
Na_2S	—	3.95×10^{-13}	—	7.43×10^{-19}
NaOS	—	8.35×10^{-6}	—	4.04×10^{-8}
$NaSO_2$	—	8.90×10^{-5}	—	5.32×10^{-7}
Na_2SO_4	2.24×10^{-11}	2.09×10^{-11}	1.87×10^{-19}	1.75×10^{-19}
NaCl	4.40×10^{-2}	3.92×10^{-2}	6.82×10^{-2}	6.07×10^{-2}
$NaCl_{(con)}$	—	2.39×10^{-3}	—	3.70×10^{-3}
$(NaCl)_2$	4.61×10^{-8}	4.95×10^{-8}	1.09×10^{-7}	1.17×10^{-7}
$(NaCl)_3$	7.27×10^{-15}	1.41×10^{-14}	2.61×10^{-14}	5.06×10^{-14}
K	5.81×10^{-3}	7.20×10^{-3}	2.27×10^{-7}	7.63×10^{-4}
K_2	2.30×10^{-12}	1.75×10^{-12}	3.43×10^{-21}	5.10×10^{-16}
KO	2.36×10^{-9}	2.76×10^{-9}	9.18×10^{-14}	5.92×10^{-12}
KO_2	—	8.29×10^{-13}	—	4.71×10^{-15}
K_2O	2.90×10^{-14}	2.50×10^{-14}	4.32×10^{-23}	3.93×10^{-22}
KS	7.07×10^{-6}	1.28×10^{-6}	2.73×10^{-10}	1.29×10^{-10}
KS_2	—	2.53×10^{-6}	—	9.19×10^{-9}
K_2S	3.14×10^{-11}	1.50×10^{-11}	4.64×10^{-20}	2.77×10^{-20}
KSO_2	—	1.70×10^{-5}	—	2.10×10^{-7}
K_2SO_4	9.08×10^{-13}	8.35×10^{-13}	1.32×10^{-21}	1.22×10^{-21}
KCl	1.06×10^{-2}	9.24×10^{-3}	6.82×10^{-3}	5.95×10^{-3}
$KCl_{(con)}$	—	3.91×10^{-4}	—	2.52×10^{-4}
$(KCl)_2$	2.24×10^{-9}	2.42×10^{-9}	9.18×10^{-10}	9.90×10^{-10}
KNa	1.80×10^{-10}	1.15×10^{-10}	6.46×10^{-19}	3.26×10^{-15}

Note. Only neutral species containing alkali or halogen elements are included in the table. Mixing ratios represent the column density of the constituent divided by the column density of SO_2. The subscript (*con*) refers to the condensed phase, "Initial" refers to the thermochemical equilibrium calculations, "Final" refers to the steady-state photochemical model results. Mixing ratios of "—" indicate that the constituent was not included in the theoretical calculations. In the sodium-enriched case, SO_2 has an initial mole fraction of 71.4% and a final mole fraction of 68.6%. In the chlorine-enriched case, SO_2 has an initial mole fraction of 70.1% and a final mole fraction of 67.4%. The final SO_2 column density is 7.66×10^{16} cm^{-2} for the sodium-enriched case and 7.55×10^{16} cm^{-2} for the chlorine-enriched case.

5. TEMPORAL EVOLUTION

The steady-state models presented in Sections 3 and 4 will not truly represent a volcanic atmosphere on Io because Io's volcanic input is not uniform, steady, and continuous across the surface or with time, because complex dynamical effects such as rapid flow away from the volcanic vents will complicate the situation (see Ingersoll 1989, Moreno *et al*. 1991), and because time-variable effects, such as diurnal changes in the solar zenith angle, will alter the production and loss rates for the different species. We now develop some time-variable models to examine how rapidly the volcanic gases are processed by photochemistry; we then compare photochemical time constants with other time scales of interest.

In our first time-variable model, we trace the rate of photochemical processing of the volcanic gases starting from the uniformly mixed thermochemical equilibrium abundances listed in Table I. One assumption of our thermochemical equilibrium calculations (and those of Zolotov and Fegley 2000) is that the abundances of SO_2, S_2, SO, and S seen in the Pele plume region by Spencer *et al*. (2000) and McGrath *et al*. (2000) are representative of the state of the volcanic vapors within the shallow magma chamber, lava lake, and/or volcanic conduit. If photochemical processing is very rapid after the gases are emitted, then this assumption could be suspect. In Paper 1, we determined that the time scales for photochemical processing of SO_2, S_2, and SO are long compared with ballistic lifetimes within a large plume eruption (∼20 min for an assumed initial ejection velocity of 1 km s^{-1}) or with possible dynamical time scales of gas flow away from the vent (∼17 min for an assumed horizontal length scale L of 100 km and a flow speed of 100 m s^{-1}; see Ingersoll 1989). Therefore, SO_2, SO, and S_2 are expected to survive a plume eruption in abundances relatively unaltered by photochemistry, and the observed abundances of these species in the Pele plume should be reliable indicators of conditions within the volcanic construct. The abundance of atomic sulfur, however, can change very rapidly due to photochemical processing, and the observed S abundances should be interpreted with caution. Because future plume observations may include the detections of alkali and halogen species, we now take a look at the time variability of the important sodium-, potassium-, and chlorine-bearing constituents.

Figure 8 shows the temporal variation of the column densities of some of the important alkali and chlorine species in our moderate-density model. At time zero, the atmosphere is assumed to be composed of Pele-type volcanic gases in the relative abundances listed in the "Initial" column in Table I (see also Paper 1); the constituents are assumed to have initial profiles that are uniformly mixed with height. We then allow all species to be affected by photochemistry, eddy and molecular diffusion, and condensation exactly as in our standard moderate density model. That is, the solar zenith angle is kept fixed at 60°, ultraviolet fluxes relevant to low solar activity are adopted, and the eddy diffusion coefficient is fixed at 10^9 cm^2 s^{-1} at all

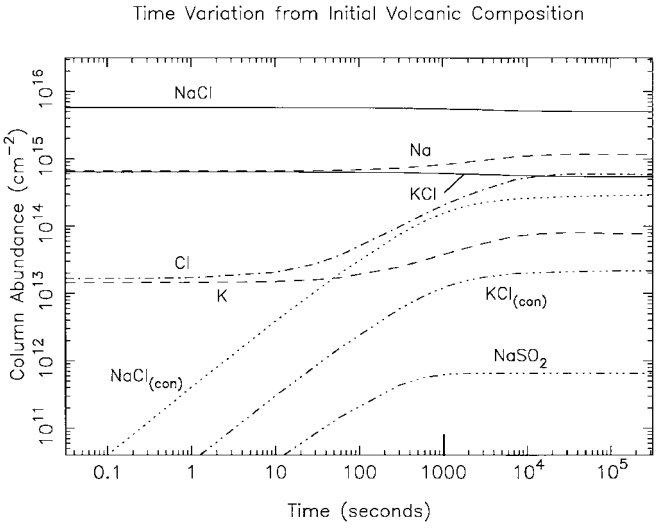

FIG. 8. The photochemical evolution of volcanic gases in our standard moderate-density model. Each curve illustrates how photochemical processes affects the column density of a major sodium-, potassium-, or chlorine-bearing constituent (as marked) in the model from its assumed initial thermochemical equilibrium abundance at time zero. The thick vertical line segment near 1000 seconds illustrates the typical dynamical time scales for a large plume eruption on Io.

altitudes. After a sufficient amount of time, the concentrations will approach the steady-state results shown in Fig. 1. Several of the constituents, however, undergo considerable changes in abundance at intermediate times (Fig. 8). For example, Fegley and Zolotov (2000) showed that at high magma temperatures and low vent pressures, such as were derived for the Pele region by Zolotov and Fegley (2000), condensed NaCl and KCl are not major thermochemical equilibrium constituents. At conditions relevant to the bulk of Io's atmosphere (or to conditions within the plume just after eruption), however, NaCl and KCl vapor can condense via homogeneous nucleation or via heterogeneous nucleation about other solid plume particles. The abundance of condensed NaCl and KCl thus increases dramatically with time in our photochemical model, while the abundances of vapor-phase NaCl and KCl decrease with time. Atomic Na, K, and Cl show secular increases due to photolysis of NaCl and KCl. Other species such as $NaSO_2$, NaS, and NaS_2 that are not included in the thermochemical equilibrium calculations (because of insufficient thermodynamic information) increase dramatically as they are synthesized by photochemical reactions.

The photochemical time constants (as defined by the column density of the constituent divided by the difference between the column-integrated photochemical production and loss rates) for the species in the initial model are 1.9 h for KCl vapor, 1.9 h for NaCl vapor, and 24 min for atomic Na. These time constants are comparable to the dynamical time scales of interest (see above), and some small amount of photochemical processing of these vapors within the plume might be expected (cf. Fig. 8). Atomic potassium and atomic chlorine have a ∼4 min and ∼30 s photochemical time constant, respectively, and any observations of Cl and K within a plume eruption should not be used to constrain the initial conditions within the volcanic vent, lava lake, or magma chamber.

In the second time-variable model, we trace the rate of loss of the volcanically produced gases once the volcanic emission has ceased. We begin with the steady-state results from our standard moderate density model, but we then change the boundary conditions such that there is no volcanic source at the bottom boundary. Sulfur dioxide is still assumed to have a fixed mixing ratio of 0.772 at the lower boundary (e.g., SO_2 frost sublimation can still occur), but all other constituent are assumed to be lost at the lower boundary at their maximum possible rates (see Paper 1). Figure 9 demonstrates that all the alkali and chlorine species in our standard moderate-density model will disappear on relatively short time scales once the volcanic sources are shut off. The photochemical time constants for Na, K, Cl, NaCl, KCl, and $NaSO_2$ in our steady-state model are 52 min, 26 min, 25 min, 1.8 h, 1.8 h, and 5.6 min, respectively. However, the rate of removal of these species from the atmosphere also depends on diffusion, and the evolutionary profiles shown in Fig. 9 reflect the diffusion time constants as well as the photochemical lifetimes. Eddy diffusion dominates near the surface, and molecular diffusion dominates at high altitudes.

The alkali and chlorine species are completely removed from the atmosphere in less than 24 hours. Sputtering at Io's surface might allow some Na, K, and Cl species to be reinjected into the atmosphere, especially in specific low-density regions (such as in nonvolcanic regions on the night side) or at specific times when the total atmospheric column density is low (e.g., total column density $\lesssim 10^{16}$ cm^{-2}; see Spencer and Schneider 1996, Pospieszalska and Johnson 1992, McGrath and Johnson 1987, Sieveka and Johnson 1985). If Na or some of the other gases

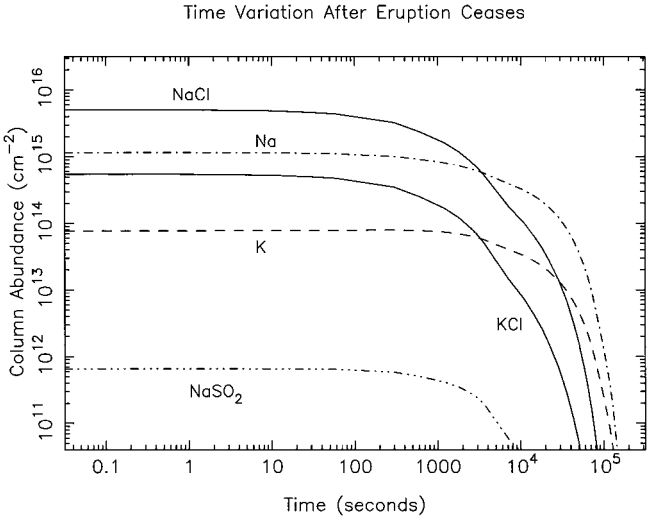

FIG. 9. The photochemical evolution of important Na-, K-, and Cl-bearing constituents in our standard moderate-density model after volcanic sources are turned off (at time zero). The curves represent the column densities of different constituents (as marked) at various points in time after the volcanic input is eliminated.

are simply adsorbed at the surface rather than being chemically bound, they might possibly be reinjected into the atmosphere along with SO_2 molecules when the sulfur dioxide frost evaporates (see Anderson *et al*. 1999, Wong and Smyth 2000). Species such as NaCl and KCl that have stable condensed phases with low vapor pressures at typical ionian temperatures may be less likely to reenter the atmosphere through this desorption process. On the other hand, NaCl and KCl might be decomposed by high-energy electrons and ions that penetrate all the way to Io's surface (e.g., Wong and Johnson 1996b), and atomic Na, K, and/or Cl might be released during this sputtering process. Therefore, observations of neutral alkali and halogen *atoms* in Io's near-surface atmosphere might not point to a specific source (i.e., volcanic vs sputtering or desorption), but observations of intact gas-phase NaCl and KCl *molecules* (i.e., at near-ultraviolet or microwave wavelengths) should provide evidence for active volcanism on Io at the time of the observations.

For our third time-variable model, we trace the diurnal variation of the atmospheric constituents in our standard Pele-type volcanic atmosphere. In this model, the volcanic sources (and total atmospheric density) are assumed to be constant with time, but photochemical processes are allowed to vary as the solar zenith angle changes during the course of an ionian day ($\sim$42 h). The boundary conditions are kept the same as in our standard moderate-density model, and the calculations are performed for the equatorial region at vernal or autumnal equinox. Figure 10 shows how the column densities of the major sodium, potassium, and chlorine species change over a daily cycle. Note that NaCl, which has a large and constant volcanic source regardless of the time of day, exhibits only small diurnal changes. Although the photolysis lifetime for NaCl in our moderate-density model is $\lesssim$ 4 h (see Table A1 in the Appendix), vertical transport times are short in the lower atmosphere where the NaCl is concentrated, and volcanic supply of NaCl controls the column density throughout the day. Because small changes in the NaCl abundance can lead to larger changes in the Na and Cl abundances (because photolysis of the more abundant NaCl molecules is the primary production mechanism), atomic sodium and chlorine exhibit more pronounced diurnal changes, and the changes are in the opposite direction from those for NaCl (i.e., more Na and Cl are produced during the day than at night). The behavior of KCl mimics that of NaCl, and K mimics that of Na and Cl. The three most abundant alkali and chlorine species, NaCl, Na, and KCl, do not have large diurnal variations, and any future observations of these constituents in plumes should not show major dawn–dusk asymmetries if solar photons are the most important dissociation agents for the NaCl and KCl (and if volcanic output is constant with time and space).

The diurnal variation of some of the ions in our moderate-density model is shown in Fig. 10b. Long-lived atomic ions such as Na^+ and K^+ (whose parent atoms show relatively little diurnal variation) exhibit much less diurnal variation than the short-lived molecular ions. Molecular ions produced from photoionization will be almost completely absent from the nightside of Io; however, torus electrons (and ions) can still contribute to ionization on the nightside, and such effects have not been included in this model.

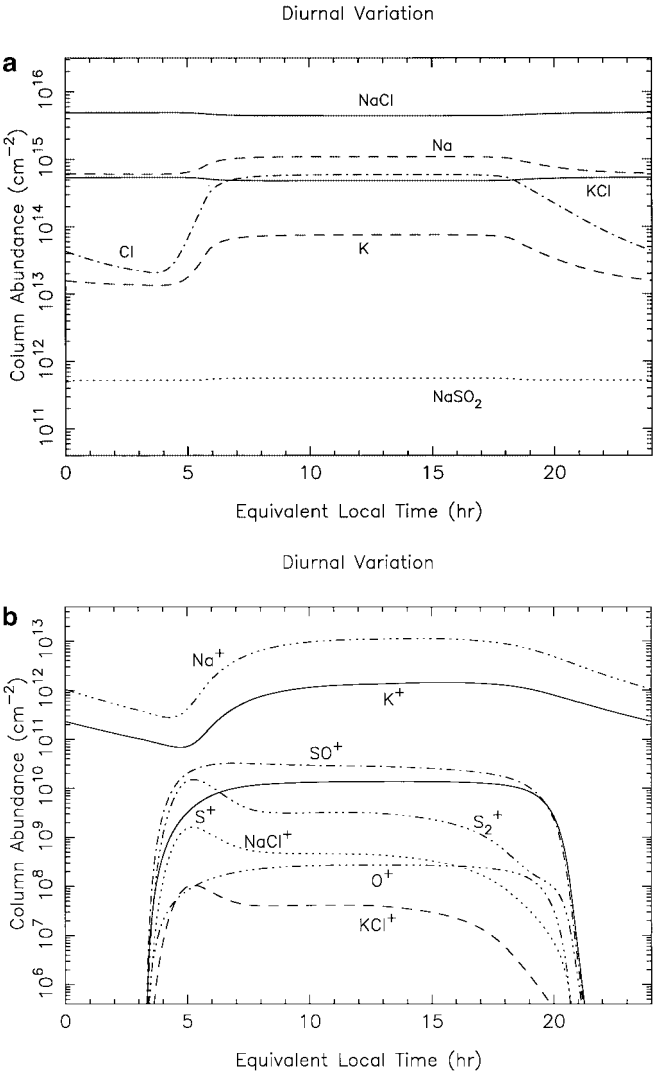

FIG. 10. The diurnal variation of important Na-, K-, and Cl-bearing constituents in our moderate-density model: (a) neutral species, (b) ions. The mixing ratios at the lower boundary (i.e., the volcanic sources) and the total atmospheric density are assumed to be constant with time, and all variations are due to photochemical processes. Column densities for the important sodium, potassium, and chlorine species (as marked) are plotted as a function of local time (at the equator at vernal or autumnal equinox), such that a local time of 0 represents midnight and 12 represents noon. Photoionization is the only ionization source in the model.

6. IMPLICATIONS FOR IO'S NEUTRAL SODIUM CLOUDS

Atoms and molecules that escape from Io form an extended cloud of neutral species that can be seen both within the vicinity of Io and out to distances of many jovian radii (see the reviews of Thomas 1992, Spencer and Schneider 1996). Although sodium species make up only a small fraction of the material that is escaping from Io, sodium atoms are very efficient at resonant scattering of solar radiation, and Io's neutral sodium clouds are

readily observable from ground-based telescopes (e.g., Brown 1974, Trafton *et al.* 1974). The most extensively observed feature of the sodium clouds is an elongated banana-shaped region ∼2–3 jovian radii in width and ∼6–8 jovian radii in length asymmetrically located near Io, but extending up to 60° in front of the satellite along its orbit around Jupiter. This "banana" cloud (also called the B cloud) is believed to result from low-speed (e.g., a few km s^{-1}) ejection of Na from sputtering of Io's atmosphere or surface (e.g., Matson *et al.* 1974, Haff *et al.* 1981, Smyth and Combi 1988, 1997).

Other observations of the jovian system indicate that very high-speed sodium (tens of kilometers per second) is being ejected from Io (see Thomas 1992 and references therein). Spencer and Schneider (1996) categorize the high-velocity features into (1) a downstream "spray" of fast sodium atoms produced when Na^+ ions in the torus undergo resonant charge exchange with neutral Na in the Io atmosphere, (2) a "sheet" or "stream" of fast sodium atoms ejected tangentially from the direction of motion of fresh pickup ions; this feature may be produced from dissociation or dissociative recombination of molecular ions that were recently ejected from Io (Schneider *et al.* 1991b, Wilson and Schneider 1994, Johnson 1994), and (3) "directional features" or "jets" produced by prompt neutralization of torus pickup ions very near Io (e.g., Spencer and Schneider 1996), by neutralization of atmospheric sodium ions that were driven radially outward from Io by Pedersen currents in Io's ionosphere (e.g., Wilson and Schneider 1999), or by atmospheric Na atoms ejected by single elastic collisions with corotating torus ions (e.g., Pilcher *et al.* 1984, Sieveka and Johnson 1984). These features are often as bright as the B cloud, and all three might contribute to an extended disk of sodium atoms seen more than 400 jovian radii from the Jupiter system (e.g., Mendillo *et al.* 1990).

6.1. Low-Speed Sodium: Corona and B Cloud

Models of Io's extended sodium corona and banana-shaped B cloud indicate that low-speed atomic sodium is being lost from Io (and supplied to the corona and B cloud) at a rate of $\sim(0.7 - 2) \times 10^{26}$ atoms s^{-1} (e.g., Murcray and Goody 1978, Pilcher *et al.* 1984, Smyth and Combi 1988, 1997, Cremonese *et al.* 1998). Observations taken over the past few decades indicate that the B cloud is remarkably stable over long time periods (see Schneider *et al.* 1989, Thomas 1992, and references therein), although a long-term increase in the inferred Na supply rate of 0.18×10^{26} atoms s^{-1} per year from 1990 to 1994 might be indicated from the data and modeling of Cremonese *et al.* (1998), and variations of up to a factor of 2 were observed in the 1970s (Bergstrahl *et al.* 1975). The ultimate source of the low-speed sodium that populates the corona and B cloud is currently believed to be sputtering of atmospheric sodium by a cascade of ion–neutral and neutral–neutral collisions caused by the interaction of corotating torus ions with atmospheric constituents (e.g., Haff *et al.* 1981, Smyth and Combi 1988, 1997).

In our simple one-dimensional model, we have not attempted to accurately account for atmospheric escape. However, we have assumed that the escape rate at the upper boundary is constrained by its limiting flow rate (see Chamberlain and Hunten 1987 for more details), so that the loss rate of a minor species such as Na cannot exceed our derived upward flux at the upper boundary of our model. The upward flux of atomic sodium at the upper boundary is 1.2×10^{10} atoms cm^{-2} s^{-1} (relative to the surface; see Table V) in our moderate-density model and 9.3×10^9 atoms cm^{-2} s^{-1} in our low-density model. If our model atmospheres were to uniformly cover Io's surface, then the predicted global escape rate for atomic sodium would be $\sim 5 \times 10^{27}$ atoms s^{-1} for the moderate-density model and $\sim 4 \times 10^{27}$ atoms s^{-1} for the low-density model. These values are ∼20–70 times higher than is indicated by the B cloud modeling discussed above. Therefore, although our boundary fluxes are not truly escape fluxes, it seems that we have either too much atomic sodium in our models or too high an eddy diffusion coefficient; alternatively, a low- or moderate-density atmosphere as described in this paper cannot uniformly cover Io's surface (i.e., the atmosphere must be patchy or dynamical effects must be considered; see Wong and Smyth 2000 for a discussion of the latter possibility).

The conclusion that our models generate too much high-altitude Na is also indicated by the observations of Schneider *et al.* (1991a), who used mutual satellite eclipses to measure the structure of Io's sodium corona. The Na density inferred from the Schneider *et al.* observations is shown in Fig. 11 (dotted curve) along with the Na profile derived from our moderate-density model (solid curve) and low-density model (dot-dashed curve). Because optically thick cold sodium would not have been readily apparent in the Schneider *et al.* data, we also include in Fig. 11 the upper limit imposed by Schneider *et al.* (1991a) for all possible sodium, including any cold Na. Note that although

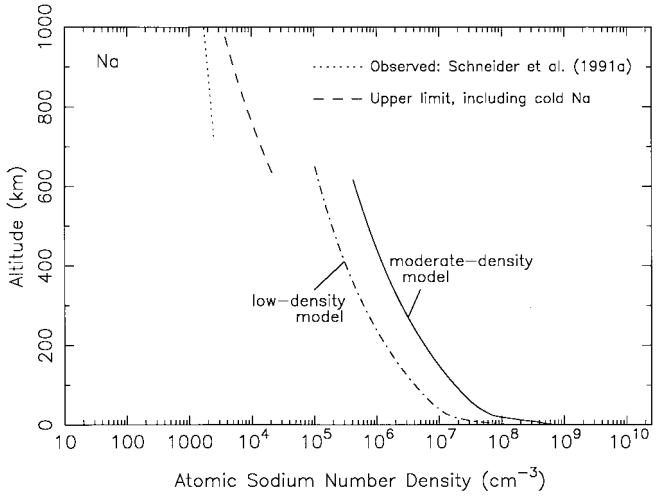

FIG. 11. The altitude profile of the sodium concentration in our moderate-density model (solid line) and low-density model (dot-dashed line) as compared with the Na corona observations of Schneider *et al.* (1991a) (dotted and dashed lines).

our sodium profile does not extend to as high altitudes as the observations of Schneider *et al*. (and our assumption of hydrostatic equilibrium certainly breaks down at high altitudes), a simple extrapolation of our model profiles would indicate Na densities one to two orders of magnitude higher than the densities observed by Schneider *et al*. at 1.4 ionian radii from the satellite's center. Part of the problem could be our neglect of torus ion and electron impact, which could allow Na densities to be depleted at high altitudes, or an overestimation of the atmospheric temperatures (and thus Na scale heights) on Io, but the obvious interpretation would be that our volcanic models do not represent global conditions across Io.

The two-dimensional photochemical and hydrodynamic models of a frost sublimation-driven atmosphere on Io presented by Wong and Smyth (2000) provide a better fit to the Schneider *et al*. (1991a) observations, although they, too, indicate a sodium column density at the exobase that is as much as a factor of 10 higher than the extrapolation of Schneider *et al*. (1991a). The Wong and Smyth (2000) and Wong and Johnson (1996a) models clearly demonstrate that dynamical processes on Io cannot be ignored. The Na column density can drop by many orders of magnitude as the gas flows away from the source region (i.e., the subsolar point in the case of a frost sublimation atmosphere or plumes in the case of a volcanic atmosphere; see also Ingersoll 1989, Moreno *et al*. 1991, Austin and Goldstein 1996, 2000), and the atmospheric Na abundance would therefore be dependent on the proximity to the source region. If Na atoms adsorb on the surface of SO_2 frost grains, then Na may be released as the SO_2 sublimates (evaporates) in sunlight. The models of Wong and Smyth (2000) then indicate that the Na column density will be much smaller on the nightside than on the dayside of a pure SO_2 frost sublimation-driven atmosphere. Support for the suggestion that Na is released when SO_2 sublimates is provided by Anderson *et al*. (1999), who observed an increase in the sodium column density in Io's vicinity as Io emerged from eclipse behind Jupiter and became sunlit again. Therefore, volcanic activity may not be the only mechanism releasing sodium from Io's surface (although volcanism is the ultimate source of sodium being released from the crust and interior).

The long-term stability of the B cloud suggests that the source of the low-speed sodium is relatively constant over long time scales. Sputtering from an atmosphere that is always collisionally thick everywhere may provide the best explanation for the apparent stability of the cloud (e.g., Schneider *et al*. 1989), and frost sublimation seems to hold the most promise for generating an atmosphere that is stable over long time periods. However, day–night asymmetries in a frost sublimation-driven atmosphere are profound (Wong and Smyth 2000), especially for condensible species such as Na, and frost sublimation atmospheres therefore seem to violate the inferred isotropic (or at least longitudinally symmetric) nature of the low-speed Na source (e.g., Smyth and Combi 1988, 1997, Schneider *et al*. 1989, Thomas 1992). We note that many of the smaller plumes (e.g., Prometheus) appear to be long lived on Io (e.g., McEwen *et al*. 1998) and could represent a relatively continuous source of sodium vapor. The gas composition in Prometheus-type plumes could differ from that of our Pele-type plume model (e.g., McEwen and Soderblom 1983, Zolotov and Fegley 1999). High-resolution Galileo images of Io (McEwen *et al*. 2000) suggest that the Prometheus-type plumes are generated when high-temperature silicate lava flows come into contact with SO_2 frost and other volatile surface deposits. Deposits of condensed NaCl, Na_2S, Na_2SO_4, or other sodium compounds could be vaporized by lava flowing across the surface. However, volcanic sources of atmospheric gas, whether from plume eruptions or lava flows across the surface, might be expected to be variable on long time scales.

Eclipse observations of Io from Earth-based telescopes at ultraviolet and visible wavelengths (e.g., Roesler *et al*. 1999, Bouchez *et al*. 2000, Scherb and Smyth 1993) and the Galileo spacecraft at visible wavelengths (McEwen *et al*. 1998, Geissler *et al*. 1999) suggest that atomic sodium has both a volcanic and nonvolcanic source on Io. In the Galileo images, diffuse green emissions believed to be caused by excitation of atomic sodium (Bouchez *et al*. 2000, Geissler *et al*. 1999) are seen in localized regions near known volcanic centers and in much broader regions across the entire the surface of the satellite, especially in nighttime images (McEwen *et al*. 1998, Geissler *et al*. 1999). If the green emissions are indeed due to sodium D lines (and not to a forbidden oxygen line at 5577 Å; see Geissler *et al*. 1999, Bouchez *et al*. 2000), then the nighttime enhancement is puzzling (cf. Fig. 10). Perhaps surface sputtering is important at night, or perhaps energetic torus electrons (and/or ions) are penetrating deeper into the atmosphere at night where they can encounter and dissociate heavier molecular sodium species, which tend to be concentrated at lower altitudes. Galileo images taken at various points in time as Io enters into eclipse indicate that the disk-averaged emission decreases with time while the localized "volcano glows" increase in intensity (Geissler *et al*. 1999). This behavior is consistent with the possible collapse of a sublimation atmosphere at night and the correspondingly deeper penetration of torus electrons in the plume-generated local atmospheres (Geissler *et al*. 1999, Wong and Smyth 2000).

In summary, from comparing our photochemical models with various Na cloud observations, we find that a global Pele-type volcanic atmosphere (even with our low-density case) is inconsistent with observations and models of the neutral sodium corona and B cloud. In order to be consistent with the inferred escape rate of slow sodium from Io, dense Pele-type atmospheres can only populate a small fraction of Io's surface. Both volcanic emission and release of Na during SO_2 frost sublimation may contribute to a lower density global atmosphere that can interact with the Io plasma torus and lead to the escape of low-speed atomic Na via atmospheric sputtering. However, we still do not understand many aspects of the problem, including the ultimate source of atmospheric Na, its observed diurnal behavior, possible long-term variations in its source strength(s), or model parameters such as the efficiency of condensation of volcanic NaCl, so the above conclusions are speculative.

6.2. *High-Speed Sodium: Molecular-Ion-Produced "Stream"*

The observed morphology and inferred velocity distribution of the "stream" feature observed by Schneider *et al.* (1991b) are consistent with fresh molecular ions NaX^+ (where X is any atom or molecular fragment) being the originator of the fast Na (Schneider *et al.* 1991b, Wilson and Schneider 1994). In this process, NaX^+ ions are presumably created near Io either from charge-exchange reactions of torus ions with neutral NaX molecules in Io's exosphere or from reactions of other molecular ions (e.g., SO^+, SO_2^+, S_2^+) with atomic Na in Io's exosphere (Johnson 1994). These NaX^+ ions then dissociate or dissociatively recombine near Io (and up to 8 h downstream from Io) to produce the peculiar morphology of the fast Na "stream" (Schneider *et al.* 1991b, Wilson and Schneider 1994, Johnson 1994). Models of the stream feature indicate that fast sodium atoms from this process are being created at a rate of $\sim 2 \times 10^{26}$ atoms s^{-1} (Schneider *et al.* 1991b), a rate comparable to the escape rate of the low-speed Na atoms that form the corona and B cloud (see above). However, the supply rate for the stream feature appears more temporally variable than that for the B cloud (e.g., Wilson and Schneider 1994). Interestingly, Mendillo *et al.* (1999) show that the variability of the stream feature in the years 1994 to 1996 can be correlated with volcanic activity on Io—the feature appears more prominent during periods of above-normal volcanic activity on Io's subjovian hemisphere.

The only important neutral NaX molecule at the exobase in our models is NaCl. Volcanic production of NaCl is also expected to be important for other types of volcanism on Io, not just for Pele-type eruptions (see Fegley and Zolotov 2000). Sodium molecules such as Na_2, NaS, NaS_2, NaOS, $NaSO_2$, NaO, and NaO_2 (some of which have been considered by other photochemical modelers) are not important constituents in the upper atmosphere because of their low volcanic production rates (e.g., Fegley and Zolotov 2000), their efficient photochemical destruction mechanisms (see Section 3 and the Appendix), and their high molecular masses (which inhibit their diffusion to high altitudes). As shown in Section 4, the concentration of NaCl at the exobase of our model depends on uncertain parameters such as the atmospheric density (i.e., the rate of volcanic influx), the condensation efficiency, the eddy diffusion coefficient, and the assumed sodium elemental abundance. Making quantitative estimates of the global escape rate of NaCl on Io is therefore difficult without better constraints on these uncertain parameters. The upward fluxes of NaCl at the upper boundary in or low-, moderate-, and high-density models are 1.4×10^9, 7.2×10^8 (see Table V),

TABLE V
Boundary Fluxes in Standard Moderate Density Model

Species	Flux at bottom ($cm^{-2}\,s^{-1}$)	Flux at top ($cm^{-2}\,s^{-1}$)	Species	Flux at bottom ($cm^{-2}\,s^{-1}$)	Flux at top ($cm^{-2}\,s^{-1}$)
Cl	-3.870×10^{11}	$+7.424 \times 10^{9}$	K	-4.718×10^{10}	$+6.282 \times 10^{8}$
Cl_2	$+5.227 \times 10^{5}$	$+1.609 \times 10^{2}$	K_2	-6.744×10^{-1}	$+2.016 \times 10^{-10}$
ClO	$+4.132 \times 10^{4}$	$+1.410 \times 10^{3}$	KO	$+4.038 \times 10^{4}$	$+1.124 \times 10^{-3}$
ClOO	-2.928×10^{-2}	$+2.180 \times 10^{-8}$	KO_2	-6.529×10^{0}	$+1.216 \times 10^{-7}$
SCl	$+4.326 \times 10^{7}$	$+2.352 \times 10^{3}$	KS	$+1.596 \times 10^{8}$	$+4.079 \times 10^{-2}$
SCl_2	$+2.820 \times 10^{2}$	$+4.166 \times 10^{-5}$	KS_2	-1.724×10^{7}	$+2.145 \times 10^{-5}$
S_2Cl	-3.379×10^{6}	$+1.793 \times 10^{1}$	K_2S	$+2.663 \times 10^{0}$	$+4.890 \times 10^{-9}$
S_2Cl_2	$+2.567 \times 10^{-2}$	$+6.333 \times 10^{-18}$	KSO_2	-1.441×10^{8}	$+2.496 \times 10^{-3}$
OSCl	-1.646×10^{3}	$+4.850 \times 10^{3}$	KCl	$+7.226 \times 10^{10}$	$+2.075 \times 10^{7}$
$ClSO_2$	-1.296×10^{4}	$+3.385 \times 10^{4}$	$KCl_{(con)}$	-2.430×10^{10}	$+6.670 \times 10^{6}$
SO_2Cl_2	-2.492×10^{-1}	$+2.038 \times 10^{-2}$	$(KCl)_2$	-8.890×10^{4}	$+7.172 \times 10^{-2}$
Na	-3.312×10^{11}	$+1.231 \times 10^{10}$	KNa	-9.459×10^{0}	$+4.094 \times 10^{-9}$
Na_2	-2.121×10^{7}	$+3.341 \times 10^{-6}$	Cl^+	-2.141×10^{-2}	$+8.298 \times 10^{3}$
NaO	$+1.501 \times 10^{7}$	$+8.000 \times 10^{-3}$	Cl^-	-3.755×10^{-3}	$+4.465 \times 10^{4}$
NaO_2	-7.382×10^{1}	$+7.632 \times 10^{-7}$	Na^+	-7.681×10^{8}	$+3.525 \times 10^{8}$
Na_2O	$+3.042 \times 10^{-1}$	$+9.508 \times 10^{-7}$	Na_2^+	-9.000×10^{2}	$+8.017 \times 10^{-9}$
NaS	-1.431×10^{6}	$+8.831 \times 10^{-1}$	NaO^+	-5.677×10^{3}	$+9.725 \times 10^{3}$
NaS_2	-1.633×10^{8}	$+1.086 \times 10^{-4}$	NaS^+	-1.866×10^{3}	$+2.006 \times 10^{1}$
Na_2S	-2.806×10^{-1}	$+4.164 \times 10^{-7}$	$NaSO_2^+$	-2.553×10^{3}	$+4.091 \times 10^{-4}$
NaOS	-9.277×10^{7}	$+2.036 \times 10^{-2}$	$NaCl^+$	-2.235×10^{4}	$+2.899 \times 10^{3}$
$NaSO_2$	-1.483×10^{9}	$+1.587 \times 10^{-2}$	K^+	-8.633×10^{7}	$+3.327 \times 10^{7}$
NaCl	$+6.592 \times 10^{11}$	$+7.156 \times 10^{8}$	KO^+	-1.648×10^{2}	$+4.793 \times 10^{2}$
$NaCl_{(con)}$	-3.118×10^{11}	$+2.475 \times 10^{8}$	KS^+	-4.667×10^{1}	$+9.556 \times 10^{-1}$
$(NaCl)_2$	-7.075×10^{6}	$+9.109 \times 10^{1}$	KSO_2^+	-2.875×10^{2}	$+3.863 \times 10^{-5}$
$(NaCl)_3$	-1.306×10^{1}	$+4.128 \times 10^{-7}$	KCl^+	-2.478×10^{3}	$+8.292 \times 10^{1}$

Note. See text for further discussion. Only the most abundant alkali and halide species are included in the table. Negative fluxes are downward, positive fluxes are upward. All fluxes are relative to a square centimeter at Io's surface radius. The fluxes listed in the table are actually calculated for the middle of the bottom layer and middle of the top layer in the model (i.e., values were printed out at half grid points rather than at the boundaries themselves).

and 4.8×10^8 molecules cm^{-2} s^{-1}, which correspond to escape rates of 6×10^{26}, 3×10^{26}, and 2×10^{26} molecules s^{-1}. Note that NaCl is more abundant at high altitudes in the low-density model than in the high-density model because of the higher temperatures (and hence scale heights) in the low-density model. The loss rate of NaCl is therefore highest in the lowest density model.

Molecular sodium ions (NaX^+) are not important in our model (see Fig. 1d) because of their rapid electron recombination rates. The most abundant NaX^+ ions in our model, $NaCl^+$ and NaO^+, have low exobase abundances and escape rates at the upper boundary. However, we have neglected impact ionization from torus plasma and from photoelectrons and we have ignored the complex time-variable behavior and dynamics of the atmosphere and the torus–atmosphere interaction, and our results regarding ion densities are probably unrealistic.

In any case, our prediction that active volcanoes can supply abundant high-altitude neutral NaCl seems encouraging for the hypothesis that the NaX^+ ion needed to explain the "stream" feature derives from neutral NaX molecules in Io's corona. The correlation of the stream feature intensity with volcanic activity (Mendillo *et al*. 1999) is also consistent with this possibility. Because volcanic models tend to produce large amounts of atomic sodium along with NaCl (Fegley and Zolotov 2000), especially if the Na/Cl ratio of the exsolved volcanic gases is greater than unity, reactions of molecular torus ions with atomic Na might contribute to the stream feature as well.

6.3. High-Speed Sodium: Directional Features

The high-speed "directional features" that show sodium being ejected from the antijovian hemisphere of Io appear variable with time, and estimates of the sodium supply rates that are needed to sustain the features range from $(3–20) \times 10^{25}$ Na atoms s^{-1} (e.g., Pilcher *et al*. 1984, Smyth and Combi, 1991, 1997, Burger *et al*. 1999, Wilson and Schneider 1999). Early model–data comparisons of the directional features (e.g., Pilcher *et al*. 1984, Sieveka and Johnson 1984) suggested that the features were caused by elastic collisions between corotating torus ions and neutral atmospheric sodium atoms. If so, the narrowness of the features and their consistent antijovian direction would imply a relatively localized, nonisotropic source (e.g., Pilcher *et al*. 1984, Smyth and Combi 1991, 1997, Burger *et al*. 1999, Wilson and Schneider 1999). Although a source from discrete active volcanoes might explain the narrowness of the features, Wilson and Schneider (1999) emphasize that the mechanism proposed by the early modelers cannot explain the consistent antijovian direction observed for these features (e.g., Pilcher *et al*. 1984, Burger *et al*. 1999) or the very high speeds ($\lesssim$80 km s^{-1}) inferred in high-resolution spectra of these features (Cremonese *et al*. 1992). Wilson and Schneider (1999) suggest that there is a region of enhanced escape in Io's antijovian hemisphere caused by preferential outward ion motion (i.e., parallel to the local electric field) in the collisionally thick portion of Io's antijovian ionosphere.

Our ionospheric model is too simplistic to address this issue or to shed much light on the possible source ion (Na^+ vs. $NaCl^+$) for this process. However, we do note that time-variable volcanic emissions can cause variations in the amount of Na, Na^+, NaCl, and $NaCl^+$ in Io's atmosphere, which in turn might affect the proposed ejection mechanisms. One might therefore expect to see correlations between the directional features and volcanic activity on the antijovian hemisphere (see the Mendillo *et al*. 1999 conclusions regarding the "stream" feature observations seemingly being correlated with volcanic activity). We also note that if photoionization were the dominant mechanism for producing the pickup ions needed for the Wilson and Schneider process, one might expect to see pronounced variations with orbital phase, as dayside ion densities are larger than nightside densities (see Fig. 10b)—ejection rates from the Wilson and Schneider mechanism would therefore peak near orbital phases of 180°, when then antijovian hemisphere is in direct sunlight (Wilson and Schneider 1999). No evidence for such longitudinal variations is observed by Wilson and Schneider (1999).

7. IMPLICATIONS FOR SURFACE COMPOSITION

Although alkali and chlorine species constitute a small percentage ($\sim$4%) of the gases in our standard model, many of these species can adsorb or condense at Io's surface and could affect surface properties. The possibility of salts such as NaCl being present on the surface of Io was proposed decades ago (e.g., Fanale *et al*. 1974, 1977) to explain several aspects of Io's visible and near-infrared spectrum. In these pre-Voyager studies, active volcanism was not considered, and the salts were suggested to have been supplied to the surface by migration of salt-saturated aqueous solutions, followed by the loss of hydrogen to space. Now that active volcanism is known to cause rapid resurfacing on Io and H_2O is known to be exceedingly rare, salt deposits are still viable surface constituents, but the likely source is silicate volcanism rather than aqueous solutions (e.g., Fegley and Zolotov 2000). Solid NaCl and KCl might form from the condensation of volcanic vapor near the sites of active plume eruptions on Io. Both NaCl and KCl are transparent (white) and have few spectral features at near ultraviolet, visible, and infrared wavelengths from $\sim$0.3 to 17 μm. These species may be detectable in the solid phase from broad spectral features in the mid-to-far infrared ($>$17 μm). Solid NaCl and KCl have very strong vibrational bands at 38–60 μm (for NaCl) and 46–68 μm (for KCl), but the bands are extremely broad and may be difficult to uniquely identify (e.g., Farmer 1974).

Crystalline NaCl and KCl can be colored by introducing impurities into the lattice structure or by bombarding the crystals with charged particles or high-energy electromagnetic radiation. These processes can create color centers, or lattice defects that cause absorption at visible wavelengths (e.g., Kittel 1976). As explained by Kittel, one of the most common types of color centers, the *F* center, arises when an electron fills a negative-ion

vacancy. For NaCl, *F* centers create an absorption feature centered at 465 nm (causing laboratory samples to appear orange colored) and for KCl, *F* centers create an absorption feature centered at 563 nm (causing samples to appear violet, purple, or magenta) (Greenwood 1970). Several researchers have suggested that surface salt deposits that are being impacted by jovian magnetospheric ions could help explain certain aspects of Io's visible reflectance spectrum such as the ~560-nm absorption feature (e.g., Fanale *et al*. 1974, 1977, Nash and Fanale 1977, Nelson and Hapke 1978). Although the production of color centers in NaCl or KCl is unlikely to be important in fresh plume deposits because of their lack of exposure to defect-causing radiation, salts in older terrains might be more affected by charged-particle bombardment, especially in the polar regions and on the trailing side of the satellite. Because visible spectra are not very diagnostic, a definitive identification of "irradiated" NaCl or KCl on Io would be difficult.

Sodium–sulfur molecules are not very important atmospheric constituents in our model. Sodium sulfate (Na_2SO_4) is a minor constituent in the volcanic gases for the conditions relevant to Pele-type eruptions (see Table I and Zolotov and Fegley 2000), and we could conceive of no photochemical production mechanisms in Io's tenuous atmosphere that would enhance its initial abundance. Because sodium sulfide (Na_2S) is more likely to be found in the condensed phase for the thermochemical equilibrium conditions derived for a Pele-type eruption (see Zolotov and Fegley 2000, Fegley and Zolotov 2000), Na_2S is also not an important vapor-phase constituent in the initial plume gas. Some photochemical production of Na_2S does occur in our model, but the production is not very efficient. However, solid or liquid Na_2S particles might be ejected during plume eruptions, and these particles could affect surface spectral properties.

The dominant sulfur–chlorine molecule produced photochemically in our model is S_2Cl. Fegley and Zolotov (2000) discuss volcanic production of other sulfur–chlorine molecules that might be produced under different thermochemical equilibrium conditions. From laboratory investigations of the spectra of sulfur–chlorine species as pure solids or diluted in SO_2 ice, Schmitt and Rodriguez (2000) and Schmitt *et al*. (2001) tentatively ascribe a 2550 cm^{-1} absorption band observed locally on Io from the Galileo Near Infrared Mapping Spectrometer (NIMS) to either pure solid H_2S or to SO_2Cl_2 (sulfuryl chloride) diluted in solid SO_2. Schmitt and Rodriguez (2000) suggest that diluted SO_2Cl_2 might also help explain a 587 cm^{-1} emission feature observed by the Voyager Infrared Interferometer Spectrometer (IRIS). Sulfuryl chloride is not a major constituent in the thermochemical equilibrium calculations of Fegley and Zolotov (2000) for Pele-type eruption conditions (see Table I), even for high assumed Cl/Na ratios in the volcanic gases (see Table IV; note, however, that lower temperature, higher pressure, and higher assumed Cl/S ratio volcanic conditions can lead to moderately increased thermochemical equilibrium abundances of SO_2Cl_2). Gas-phase photochemical processes can enhance the SO_2Cl_2 abundance (see Tables I and IV), but SO_2Cl_2 is never an important chlorine-bearing component in our Pele-type volcanic models (i.e., its column-integrated mixing ratio relative to SO_2 never exceeds 3×10^{-12}) despite the fact that we have tried to maximize possible production rates (by assuming high rate constants) and have purposely underestimated photolysis rates and other loss processes. The dominant production mechanism for SO_2Cl_2 in our photochemical model is reaction R462 ($2ClSO_2 \rightarrow SO_2Cl_2$), with a much smaller contribution from R363 ($Cl + ClSO_2 + M \rightarrow SO_2Cl_2 + M$). The $ClSO_2$ needed for these reactions is derived from ion chemistry (R735: $Cl^- + SO_2 \rightarrow ClSO_2 + e^-$) or from three-body reactions (R340: $SO_2 + Cl + M \rightarrow ClSO_2 + M$). The low densities of Io's atmosphere do not favor three-body reactions such as R363 and R340; thus, gas-phase production of SO_2Cl_2 is hindered on Io.

However, heterogeneous reactions may be more favorable for the production of SO_2Cl_2. In a series of laboratory investigations, Bahou *et al*. (2000) show that both $ClSO_2$ and SO_2Cl_2 can be created when a low-temperature argon or krypton matrix containing Cl_2 and SO_2 is irradiated by relatively long wavelength (308-nm) ultraviolet light. In these experiments, the production mechanism is presumably the photodissociation of Cl_2, followed by the reaction of Cl atoms with SO_2 to form $ClSO_2$, followed by the reaction of $ClSO_2$ with another chlorine atom to form SO_2Cl_2 (Bahou *et al*. 2000). If chlorine atoms (which tend to be more abundant in our models than Cl_2 molecules) in a fresh volcanic eruption can adsorb on the surface without reacting with other radicals there, then Cl may react with adsorbed SO_2 to form $ClSO_2$ and eventually SO_2Cl_2 at Io's surface. This mechanism would occur preferentially for high Cl/S and Cl/Na ratios in the exsolved volcanic gases (so the chlorine is not all tied up in NaCl) and in regions where SO_2 gas is adsorbed on the surface rather than being tied up in the solid phase (e.g., in fresh plume deposits or in "warm" areas across the surface). The fact that SO_2Cl_2 is relatively susceptible to destruction by ultraviolet radiation (for $\lambda < 360$ nm) further favors fresh plume deposits as the likely location for any SO_2Cl_2 molecules. Note that the 3.915-μm absorption feature that Schmitt and Rodriguez (2000) attribute to SO_2Cl_2 has been definitively identified only in the red plume deposits south of Marduk on Io. As is discussed by Moses *et al*. (2001), Spencer *et al*. (2000), McEwen *et al*. (1998), and others (see Paper 1), red deposits may signify relatively recent S_2-rich plume eruptions.

Some of the more volatile alkali and chlorine vapors may not be abundant enough to form distinct surface units, and the molecules or atoms may simply adsorb on surface grains. If so, these species might be released as SO_2 frost evaporates during the daytime.

8. CONCLUSIONS

Active volcanoes can supply alkali and halogen species to Io's atmosphere. From thermochemical equilibrium considerations of the likely partitioning of alkalis and chlorine in volcanic

gases generated from silicate magmas on Io (Fegley and Zolotov 2000) and from models of the likely photochemical processing of these vapors once they are released into the atmosphere (see Sections 3–5), we determine that NaCl, Na, Cl, KCl, and K will be the most important alkali and chlorine gases in atmospheres generated from Pele-like plumes on Io. The relative abundance of each of these constituents depends on uncertain quantities such as their condensation efficiency (Section 4.3), the strength of atmospheric mixing (Section 4.2), the initial Na/Cl ratio in the exsolved volcanic gases (Section 4.5 and Fegley and Zolotov 2000), and other physical and chemical conditions in the source magma (Fegley and Zolotov 2000).

The dominant photochemical loss mechanisms for NaCl and KCl are photolysis and condensation. Neither NaCl nor KCl are efficiently recycled under typical atmospheric conditions on Io, so both molecules will be depleted quickly from the atmosphere once volcanic emission ceases (unless these molecules can be reintroduced to the atmosphere by surface sputtering, micrometeoroid impact, revolatilization of surface deposits due to lava mobilization, co-evaporation as the SO_2 frost sublimates, etc.). In contrast, atomic Na, K, and Cl (whose photochemical production rates from NaCl and KCl photolysis are greater than their volcanic supply rates) are difficult to destroy by photochemical means. Atomic sodium and potassium are destroyed by three-body reactions with sulfur molecules and by ionization (potassium can also react with NaCl vapor to form KCl + Na), and chlorine atoms are destroyed predominantly by reactions with sulfur-containing molecules.

Our models suggest that NaCl vapor may be abundant enough to be observed in active plumes on Io at ultraviolet (220–280 nm) or microwave wavelengths. If so, then such observations might provide another way to monitor volcanic activity on Io. Identification of solid NaCl and KCl as surface constituents may prove more difficult due to the low overall predicted fractional coverage of these materials on the surface and to the unfavorable spectral properties of NaCl and KCl crystals (which are often used as window materials for infrared spectrometers or as reflectance standards for visible and infrared spectrometers). In older terrain, salt deposits that have been exposed to bombardment by energetic torus plasma might become more spectrally interesting due to the development of color centers (i.e., visible absorption features caused by lattice defects; see Fanale *et al*. 1974, 1977). Freshly condensed NaCl and KCl around volcanic vents should be white and bland at near-ultraviolet through mid-infrared wavelengths.

The inferred escape rate of low-speed sodium required to supply Io's sodium corona and B cloud (e.g., Spencer and Schneider 1996) is more than an order of magnitude lower than our estimate for the escape rate from a moderately dense (2 nbars) or low-density (0.37 nbar) Pele-type volcanic atmosphere (if we assume the atmosphere uniformly covers Io's surface). Although this result is somewhat sensitive to uncertain model parameters, it suggests that our simple one-dimensional photochemical models do not provide adequate descriptions of the complex behavior of Io's global atmosphere and/or that 0.37-nbar or higher density volcanic atmospheres such as the ones presented here do not cover a large fraction of Io's surface. The latter conclusion is supported by numerous observations of the SO_2 abundance on Io that suggest a "patchy" ionian atmosphere (see Lellouch 1996 for a review), and the former conclusion is supported by the more sophisticated two-dimensional frost sublimation, photochemistry, and transport models of Wong and Johnson (1996a) and Wong and Smyth (2000). The relative contributions of active volcanism, surface sputtering, and sublimation (i.e., corelease of sodium atoms or molecules during SO_2 frost sublimation) to the abundance of sodium in Io's global atmosphere remain uncertain. If the active volcanic component dominates, then the low-speed Na might be supplied from atmospheric sputtering from a small number of relatively dense volcanic plumes or from a lower density global volcanic atmosphere supplied by a large number of small plumes (in which a global atmosphere is maintained by dynamical flow away from volcanic vents; see Ingersoll 1989, Moreno *et al*. 1991). In either case, if the B cloud has a direct volcanic origin, volcanic emission on Io must be roughly constant over long time scales (years) to explain the apparent stability of the sodium B cloud (e.g., Thomas 1992, Spencer and Schneider 1996).

During periods in which active volcanism is prevalent across Io, we determine that NaCl molecules will be important constituents of Io's upper atmosphere. This result suggests that the NaX^+ ion needed to explain the observed high-velocity sodium "stream" feature (e.g., Schneider *et al*. 1991b, Wilson and Schneider 1994, Johnson 1994) could derive from volcanically produced neutral NaCl molecules in Io's exosphere/corona. The correlation of the stream feature with volcanic activity (Mendillo *et al*. 1999) is consistent with this possibility. Our modeling does not shed much light on the origin of the high-speed sodium "directional features" other than to demonstrate that active volcanism can supply abundant atmospheric sodium and to suggest that the observed variability of these features (e.g., Pilcher *et al*. 1884, Burger *et al*. 1999, Wilson and Schneider 1999) could be caused by variations in volcanic activity (both in space and in time).

The models presented here were developed to highlight the interesting photochemical reactions that might take place when active volcanoes on Io emit sodium, potassium, and chlorine vapor. The observed heterogeneity of Io's atmosphere (e.g., McGrath *et al*. 2000, Hendrix *et al*. 1999, Geissler *et al*. 1999, Roesler *et al*. 1999, Lellouch *et al*. 1992, 1994, 1996; Lellouch 1996, Ballester *et al*. 1994; Sartoretti *et al*. 1994, 1996) and theoretical studies that predict rapid dynamical gas flow away from vapor source regions on Io (e.g., Ingersoll 1989, Moreno *et al*. 1991, Wong and Johnson 1996a, Wong and Smyth 2000, Austin and Goldstein 2000) indicate that one-dimensional models will be insufficient in describing the complex multidimensional nature of Io's atmosphere. Because of the probable importance of volcanoes as atmospheric drivers, future multidimensional models of photochemistry and transport on Io should be developed

that include volcanic sources as well as SO_2 frost sublimation (cf. Wong and Johnson 1996a, Wong and Smyth 2000).

APPENDIX: PHOTOCHEMICAL REACTIONS AND CONDENSATION

The photodissociation reactions for the neutral sodium, potassium, and chlorine species in our model are listed in Table A1. The table also lists the photolysis rates (J values) in free space at 1 AU for low solar activity and the photolysis rates at 490 and 10 km in our moderate-density model. The cross sections for the chlorine-bearing species were generally taken from the Venus study of Mills (1998); cross sections for the sodium compounds were found in the literature for the Earth's upper atmosphere (Silver *et al*. 1986, Rajasekhar *et al*. 1989, Helmer and Plane 1993, Eska *et al*. 1999).

Table A2 provides the complete list of neutral reactions for the Na-, K-, and Cl-bearing species in our model. Note that the rate coefficients for many of the alkali and chlorine reactions are not well determined and had to be estimated. The kinetics databases and compilations of Mallard *et al*. (1998), DeMore *et al*. (1997), and Atkinson *et al*. (1997) were useful in creating this list, as were the flame chemistry studies of Schofield and Steinberg (1992) and Jensen and Jones (1978).

Condensation of S_8, NaCl, $(NaCl)_2$, $(NaCl)_3$, KCl, and $(KCl)_2$ about atmospheric aerosols (e.g., plume dust particles) has been included in the model. Condensation within a rapidly expanding volcanic plume is a complicated problem that we do not attempt to solve correctly. Instead, we assume that vapor can condense about preexisting atmospheric aerosol particles (condensation nuclei). The preexisting aerosols are assumed to be mixed throughout Io's atmosphere and to have a concentration profile that does not vary with time. Condensation about these aerosol particles is assumed to be diffusion-limited, with a condensation rate that depends on particle size and concentration (see Moses *et al*. 2000 for more details). Evaporation is ignored. In our standard moderate-density model, we assume that the preexisting aerosol particles have a concentration that varies as a function of altitude and is equal to 1.32×10^{-10} times the total

TABLE A1
Photolysis Reactions

		Photolysis rate J (s^{-1})				
	Reaction	at 1 AU	at 490 km	at 10 km	Wavelength (nm)	Reference
R24	$Cl_2 \xrightarrow{h\nu} 2Cl$	2.5×10^{-3}	9.4×10^{-5}	9.3×10^{-5}	$238 \le \lambda \le 475$	a
R26	$ClO \xrightarrow{h\nu} Cl + O$	6.1×10^{-3}	2.2×10^{-4}	2.1×10^{-4}	$228 \le \lambda \le 325$	a
R28	$ClOO \xrightarrow{h\nu} ClO + O$	9.5×10^{-3}	3.5×10^{-4}	3.3×10^{-4}	$218 \le \lambda \le 280$	a
R29	$OClO \xrightarrow{h\nu} ClO + O$	7.6×10^{-2}	2.8×10^{-3}	2.8×10^{-3}	$148 \le \lambda \le 435$	a
R30	$ClO_3 \xrightarrow{h\nu} ClO + O_2$	2.2×10^{-2}	8.2×10^{-4}	7.9×10^{-4}	$198 \le \lambda \le 350$	a
R31	$Cl_2O \xrightarrow{h\nu} Cl + ClO$	3.9×10^{-3}	1.4×10^{-4}	1.4×10^{-4}	$198 \le \lambda \le 505$	a
R32	$Cl_2O_2 \xrightarrow{h\nu} Cl + ClOO$	6.3×10^{-3}	2.3×10^{-4}	2.2×10^{-4}	$188 \le \lambda \le 455$	a
R33	$SCl \xrightarrow{h\nu} S + Cl$	2.5×10^{-2}	9.3×10^{-4}	9.3×10^{-4}	$335 \le \lambda \le 505$	a
R34	$SCl_2 \xrightarrow{h\nu} SCl + Cl$	2.2×10^{-3}	8.2×10^{-5}	8.1×10^{-5}	$188 \le \lambda \le 465$	a
R35	$SCl_2 \xrightarrow{h\nu} S + 2Cl$	2.8×10^{-4}	1.0×10^{-5}	8.3×10^{-6}	$188 \le \lambda \le 233$	a
R36	$S_2Cl \xrightarrow{h\nu} S_2 + Cl$	6.6×10^{-2}	2.5×10^{-3}	2.5×10^{-3}	$325 \le \lambda \le 485$	a
R37	$S_2Cl \xrightarrow{h\nu} SCl + S$	1.8×10^{-4}	6.6×10^{-6}	6.6×10^{-6}	$325 \le \lambda \le 345$	a
R38	$S_2Cl_2 \xrightarrow{h\nu} 2\,SCl$	1.1×10^{-2}	4.0×10^{-4}	3.8×10^{-4}	$178 \le \lambda \le 390$	a
R39	$S_2Cl_2 \xrightarrow{h\nu} S_2 + 2Cl$	1.2×10^{-2}	4.4×10^{-4}	4.0×10^{-4}	$108 \le \lambda \le 280$	a
R40	$S_2Cl_2 \xrightarrow{h\nu} S_2Cl + Cl$	1.4×10^{-2}	5.2×10^{-4}	5.1×10^{-4}	$228 \le \lambda \le 390$	a
R41	$SO_2Cl_2 \xrightarrow{h\nu} ClSO_2 + Cl$	—	1.0×10^{-8}	1.0×10^{-8}		Estimate
R42	$Na_2 \xrightarrow{h\nu} 2\,Na$	—	3.0×10^{-4}	3.0×10^{-4}		Est., b
R43	$NaO_2 \xrightarrow{h\nu} Na + O_2$	5.8×10^{-3}	2.1×10^{-4}	2.0×10^{-4}	$148 \le \lambda \le 325$	c
R44	$NaO_3 \xrightarrow{h\nu} NaO + O_2$	—	3.7×10^{-6}	3.7×10^{-6}		Est., d
R45	$Na_2O \xrightarrow{h\nu} NaO + Na$	—	1.0×10^{-5}	1.0×10^{-5}		Est., b
R48	$NaS_2 \xrightarrow{h\nu} Na + S_2$	—	3.2×10^{-4}	3.0×10^{-4}		Est. $= 1.5 \times J_{42}$
R49	$Na_2S \xrightarrow{h\nu} NaS + Na$	—	1.0×10^{-5}	1.0×10^{-5}		Est., b
R50	$NaCl \xrightarrow{h\nu} Na + Cl$	2.4×10^{-3}	8.8×10^{-5}	8.2×10^{-5}	$183 \le \lambda \le 285$	e
R51	$KO_2 \xrightarrow{h\nu} K + O_2$	—	2.1×10^{-4}	2.0×10^{-4}		Est., f
R54	$KCl \xrightarrow{h\nu} K + Cl$	—	1.1×10^{-4}	1.1×10^{-4}		Est. $= 1.3 \times J_{49}$

Note. Only those photodissociation reactions affecting alkali and halogen species are included in the table. The first column of J values corresponds to the photolysis rate in free space at 1 AU for low solar activity; the second and third columns correspond to the photolysis rates at 490 and 10 km altitude in our Io model for a 60° solar zenith angle and low solar activity. See Mills (1998) for details about the adopted solar flux. Although pure sulfur, oxygen, and hydrogen reactions are not included in the list, the full numbering system is maintained for consistency between papers (see Paper 1). References: (a) Mills (1998) and references therein; (b) Summers and Strobel (1996); (c) Rajasekhar *et al*. (1989); (d) Helmer and Plane (1993); (e) Silver *et al*. (1986); (f) Eska *et al*. (1999).

TABLE A2
Neutral Alkali and Chlorine Reactions

	Reaction[a]	Rate constant[b]	Reference
R79	$O + Cl \xrightarrow{M} ClO$	$k_0 = 1.0 \times 10^{-29}\, T^{-1}$	Est., Jensen and Jones (1978)
R80	$O + Cl_2 \longrightarrow ClO + Cl$	$4.17 \times 10^{-12}\, e^{(-1368/T)}$	Baulch *et al*. (1981)
R82	$O + ClO \longrightarrow O_2 + Cl$	$3.0 \times 10^{-11}\, e^{(70/T)}$	DeMore *et al*. (1997)
R84	$O + ClOO \longrightarrow ClO + O_2$	4.98×10^{-11}	Basco and Dogra (1971)
R85	$O + OClO \longrightarrow ClO + O_2$	$2.4 \times 10^{-12}\, e^{(-960/T)}$	DeMore *et al*. (1997)
R87	$O + Cl_2O \longrightarrow 2ClO$	$2.7 \times 10^{-11}\, e^{(-530/T)}$	DeMore *et al*. (1997)
R88	$O + SCl \longrightarrow SO + Cl$	1.2×10^{-10}	Murrells (1988b)
R89	$O + SCl_2 \longrightarrow SO + Cl_2$	1.0×10^{-16}	Estimate
R90	$O + S_2Cl \longrightarrow SO + SCl$	1.0×10^{-13}	Estimate
R91	$O + OSCl \longrightarrow SO_2 + Cl$	$5.0 \times 10^{-11}\, e^{(-600/T)}$	Estimate
R92	$O + OSCl \longrightarrow SO + ClO$	$2.0 \times 10^{-11}\, e^{(-600/T)}$	Estimate
R93	$O + ClSO_2 \longrightarrow SO_2 + ClO$	1.0×10^{-11}	Est., Mills (1998)
R94	$O + Na \xrightarrow{M} NaO$	$k_0 = 1.0 \times 10^{-27}\, T^{-2}$	Estimate
R95	$O + Na_2 \longrightarrow NaO + Na$	$4.0 \times 10^{-10}\, e^{(-800/T)}$	Estimate
R98	$O + NaO \longrightarrow Na + O_2$	$1.56 \times 10^{-11}\, T^{0.5}$	Plane and Husain (1986)
R99	$O + NaO_2 \longrightarrow NaO + O_2$	$5.0 \times 10^{-10}\, e^{(-940/T)}$	Helmer and Plane (1993)
R100	$O + NaO_3 \longrightarrow Na + 2O_2$	$1.77 \times 10^{-11}\, T^{0.5}$	Est., Helmer and Plane (1993)
R101	$O + Na_2O \longrightarrow 2\,NaO$	1.0×10^{-12}	Est., Summers and Strobel (1996)
R102	$O + Na_2O \longrightarrow Na_2 + O_2$	1.0×10^{-14}	Estimate
R103	$O + NaS \longrightarrow Na + SO$	3.7×10^{-10}	Assume same as O + NaO
R104	$O + NaS_2 \longrightarrow NaS + SO$	$2.0 \times 10^{-10}\, e^{(-940/T)}$	Est. based on $O + NaO_2$
R105	$O + NaS_2 \longrightarrow NaO + S_2$	$3.0 \times 10^{-10}\, e^{(-940/T)}$	Est. based on $O + NaO_2$
R106	$O + Na_2S \longrightarrow NaS + NaO$	1.0×10^{-12}	Est., Summers and Strobel (1996)
R107	$O + Na_2S \longrightarrow Na_2 + SO$	1.0×10^{-14}	Estimate
R108	$O + NaOS \longrightarrow Na + SO_2$	$3.0 \times 10^{-10}\, e^{(-940/T)}$	Est. based on $O + NaO_2$
R109	$O + NaOS \longrightarrow NaO + SO$	$2.0 \times 10^{-10}\, e^{(-940/T)}$	Est. based on $O + NaO_2$
R110	$O + NaSO_2 \longrightarrow NaO + SO_2$	$8.5 \times 10^{-10}\, e^{(-800/T)}$	Est., based on Schofield and Steinberg (1992)
R111	$O + K \xrightarrow{M} KO$	$k_0 = 1.0 \times 10^{-27}\, T^{-2}$	Estimate
R112	$O + K_2 \longrightarrow KO + K$	$4.0 \times 10^{-10}\, e^{(-800/T)}$	Estimate
R114	$O + KO \longrightarrow K + O_2$	$1.56 \times 10^{-11}\, T^{0.5}$	Est. based on O + NaO
R115	$O + KO_2 \longrightarrow KO + O_2$	$5.0 \times 10^{-10}\, e^{(-940/T)}$	Est. based on $O + NaO_2$
R116	$O + KS \longrightarrow K + SO$	$1.56 \times 10^{-11}\, T^{0.5}$	Est. based on O + NaO
R117	$O + KS_2 \longrightarrow KS + SO$	$2.0 \times 10^{-10}\, e^{(-940/T)}$	Est. based on $O + NaO_2$
R118	$O + KS_2 \longrightarrow KO + S_2$	$3.0 \times 10^{-10}\, e^{(-940/T)}$	Est. based on $O + NaO_2$
R119	$O + K_2S \longrightarrow KO + KS$	1.0×10^{-12}	Estimate
R120	$O + K_2S \longrightarrow K_2 + SO$	1.0×10^{-14}	Estimate
R121	$O + KSO_2 \longrightarrow KO + SO_2$	$8.5 \times 10^{-10}\, e^{(-800/T)}$	Est. based $O + NaSO_2$
R122	$O + KNa \longrightarrow KO + Na$	$2.0 \times 10^{-10}\, e^{(-800/T)}$	Estimate
R123	$O + KNa \longrightarrow K + NaO$	$2.0 \times 10^{-10}\, e^{(-800/T)}$	Estimate
R136	$O_2 + Cl \xrightarrow{M} ClOO$	$k_0 = 6.25 \times 10^{-24}\, T^{-2.9}$	Baer *et al*. (1991)
R137	$O_2 + SCl \longrightarrow SO + ClO$	$1.0 \times 10^{-12}\, e^{(-1400/T)}$	DeMore *et al*. (1997)
R138	$O_2 + Na \xrightarrow{M} NaO_2$	$k_0 = 9.32 \times 10^{-27}\, T^{-1.4}$	DeMore *et al*. (1997)
R139	$O_2 + NaO \xrightarrow{M} NaO_3$	$k_0 = 3.11 \times 10^{-25}\, T^{-2}$	DeMore *et al*. (1997)
R140	$O_2 + K \xrightarrow{M} KO_2$	$k_0 = 8.8 \times 10^{-27}\, T^{-1.23}$	DeMore *et al*. (1997)
R147	$O_3 + Cl \longrightarrow ClO + O_2$	$2.9 \times 10^{-11}\, e^{(-260/T)}$	DeMore *et al*. (1997)
R148	$O_3 + ClO \longrightarrow ClOO + O_2$	$2.0 \times 10^{-12}\, e^{(-4500/T)}$	Estimate
R149	$O_3 + ClO \longrightarrow OClO + O_2$	$1.0 \times 10^{-12}\, e^{(-4500/T)}$	Estimate
R150	$O_3 + Na \longrightarrow NaO + O_2$	$1.1 \times 10^{-9}\, e^{(-116/T)}$	Plane *et al*. (1993)
R151	$O_3 + NaO \longrightarrow NaO_2 + O_2$	$1.1 \times 10^{-9}\, e^{(-568/T)}$	Plane *et al*. (1993)
R152	$O_3 + NaO \longrightarrow Na + 2\,O_2$	$3.2 \times 10^{-10}\, e^{(-550/T)}$	Plane *et al*. (1993)
R153	$O_3 + K \longrightarrow KO + O_2$	$1.15 \times 10^{-9}\, e^{(-120/T)}$	Plane and Helmer (1994)
R154	$O_3 + KO \longrightarrow KO_2 + O_2$	$1.1 \times 10^{-9}\, e^{(-568/T)}$	Est. based on O_3 + NaO
R155	$O_3 + KO \longrightarrow K + 2\,O_2$	$6.9 \times 10^{-10}\, e^{(-385/T)}$	Eska *et al*. (1999)
R228	$S + Cl \xrightarrow{M} SCl$	$k_0 = 1.0 \times 10^{-29}\, T^{-1}$	Est. based on O + Cl
R229	$S + ClO \longrightarrow SO + Cl$	4.0×10^{-11}	Estimate
R230	$S + ClOO \longrightarrow SO + ClO$	4.0×10^{-11}	Estimate
R231	$S + ClOO \longrightarrow SO_2 + Cl$	4.0×10^{-12}	Estimate
R232	$S + OClO \longrightarrow SO + ClO$	4.0×10^{-11}	Estimate
R235	$S + Cl_2O \longrightarrow SCl + ClO$	$2.7 \times 10^{-11}\, e^{(-530/T)}$	Est. based on $O + Cl_2O$

TABLE A2—*Continued*

	Reaction[a]	Rate constant[b]	Reference
R236	$S + Cl_2O_2 \longrightarrow SCl + OClO$	$3.0 \times 10^{-11}\, e^{(-400/T)}$	Estimate
R237	$S + SCl \longrightarrow S_2 + Cl$	3.0×10^{-11}	Estimate
R238	$S + S_2Cl_2 \longrightarrow SCl + S_2Cl$	$3.0 \times 10^{-11}\, e^{(-1500/T)}$	Estimate
R239	$S + OSCl \longrightarrow S_2O + Cl$	$5.0 \times 10^{-11}\, e^{(-600/T)}$	Estimate
R240	$S + OSCl \longrightarrow SO + SCl$	$2.0 \times 10^{-11}\, e^{(-600/T)}$	Estimate
R241	$S + ClSO_2 \longrightarrow SO_2 + SCl$	1.0×10^{-11}	Est. based on $O + ClSO_2$
R242	$S + Na \xrightarrow{M} NaS$	$k_0 = 1.6 \times 10^{-24}\, T^{-2}$	Est., Schofield and Steinberg (1992)
R243	$S + Na_2 \longrightarrow NaS + Na$	$4.0 \times 10^{-10}\, e^{(-800/T)}$	Estimate
R246	$S + NaO \longrightarrow Na + SO$	$1.56 \times 10^{-11}\, T^{0.5}$	Est. based on $O + NaO$
R247	$S + NaO_2 \longrightarrow NaO + SO$	$4.0 \times 10^{-10}\, e^{(-940/T)}$	Est. based on $O + NaO_2$
R248	$S + NaO_2 \longrightarrow NaS + O_2$	$1.0 \times 10^{-10}\, e^{(-940/T)}$	Est. based on $O + NaO_2$
R249	$S + Na_2O \longrightarrow NaO + NaS$	1.0×10^{-12}	Est., Summers and Strobel (1996)
R250	$S + Na_2O \longrightarrow Na_2 + SO$	1.0×10^{-14}	Estimate
R251	$S + NaS \longrightarrow Na + S_2$	$1.56 \times 10^{-11}\, T^{0.5}$	Est. based on $O + NaO$
R252	$S + NaS_2 \longrightarrow NaS + S_2$	$6.8 \times 10^{-13}\, T^{0.5}$	Est., Schofield and Steinberg (1992)
R253	$S + Na_2S \longrightarrow 2\ NaS$	1.0×10^{-13}	Estimate
R254	$S + NaOS \longrightarrow NaS + SO$	$7.0 \times 10^{-13}\, T^{0.5}$	Est., Schofield and Steinberg (1992)
R255	$S + NaSO_2 \longrightarrow NaS + SO_2$	$7.2 \times 10^{-11}\, e^{(-800/T)}$	Est., based on Schofield and Steinberg (1992)
R256	$S + K \xrightarrow{M} KS$	$k_0 = 1.6 \times 10^{-24}\, T^{-2}$	Est. based on $S + Na$
R257	$S + K_2 \longrightarrow KS + K$	$4.0 \times 10^{-10}\, e^{(-800/T)}$	Estimate
R259	$S + KO \longrightarrow K + SO$	$1.56 \times 10^{-11}\, T^{0.5}$	Est. based on $O + NaO$
R260	$S + KO_2 \longrightarrow KO + SO$	$4.0 \times 10^{-10}\, e^{(-940/T)}$	Est. based on $O + NaO_2$
R261	$S + KO_2 \longrightarrow KS + O_2$	$1.0 \times 10^{-10}\, e^{(-940/T)}$	Est. based on $O + NaO_2$
R262	$S + KS \longrightarrow K + S_2$	$1.56 \times 10^{-11}\, T^{0.5}$	Est. based on $O + NaO$
R263	$S + KS_2 \longrightarrow KS + S_2$	$6.8 \times 10^{-13}\, T^{0.5}$	Est. based on $S + NaS_2$
R264	$S + K_2S \longrightarrow 2\ KS$	5.0×10^{-12}	Estimate
R265	$S + KSO_2 \longrightarrow KS + SO_2$	$7.2 \times 10^{-11}\, e^{(-800/T)}$	Est. based on $S + NaSO_2$
R266	$S + KNa \longrightarrow Na + KS$	$2.0 \times 10^{-10}\, e^{(-800/T)}$	Estimate
R267	$S + KNa \longrightarrow NaS + K$	$2.0 \times 10^{-10}\, e^{(-800/T)}$	Estimate
R276	$S_2 + ClO \longrightarrow S_2O + Cl$	2.8×10^{-11}	Est. based on $SO + ClO$
R277	$S_2 + SCl \longrightarrow S_3 + Cl$	2.0×10^{-11}	Estimate
R278	$S_2 + ClSO_2 \longrightarrow S_2Cl + SO_2$	$5.0 \times 10^{-11}\, e^{(-800/T)}$	Estimate
R279	$S_2 + Na \xrightarrow{M} NaS_2$	$k_0 = 1.6 \times 10^{-24}\, T^{-2}$	Est., Schofield and Steinberg (1992)
R280	$S_2 + NaSO_2 \longrightarrow NaS_2 + SO_2$	$6.3 \times 10^{-11}\, e^{(-800/T)}$	Est. based on Schofield and Steinberg (1992)
R281	$S_2 + K \xrightarrow{M} KS_2$	$k_0 = 1.6 \times 10^{-24}\, T^{-2}$	Est. based on $S_2 + K$
R282	$S_2 + KSO_2 \longrightarrow KS_2 + SO_2$	$6.3 \times 10^{-11}\, e^{(-800/T)}$	Est. based on $S_2 + KSO_2$
R294	$S_3 + Cl_2 \longrightarrow S_2 + SCl_2$	1.0×10^{-13}	Estimate
R295	$S_3 + SCl \longrightarrow S_4 + Cl$	1.0×10^{-13}	Estimate
R296	$S_3 + SCl \longrightarrow S_2 + S_2Cl$	1.0×10^{-13}	Estimate
R297	$S_3 + SCl_2 \longrightarrow S_2 + S_2Cl_2$	1.0×10^{-14}	Estimate
R298	$S_3 + NaS \longrightarrow S_4 + Na$	1.0×10^{-12}	Estimate
R307	$S_4 + Cl \longrightarrow S_2 + S_2Cl$	1.0×10^{-11}	Estimate
R328	$SO + Cl \xrightarrow{M} OSCl$	$k_0 = 7.3 \times 10^{-21}\, T^{-5}$	Mills (1998)
R329	$SO + ClO \longrightarrow SO_2 + Cl$	2.8×10^{-11}	DeMore *et al*. (1997)
R330	$SO + ClOO \longrightarrow SO_2 + ClO$	2.0×10^{-11}	Estimate
R331	$SO + ClOO \longrightarrow OSCl + O_2$	1.0×10^{-13}	Estimate
R332	$SO + OClO \longrightarrow SO_2 + ClO$	1.9×10^{-12}	DeMore *et al*. (1997)
R333	$SO + SCl \longrightarrow S_2O + Cl$	1.0×10^{-11}	Estimate
R334	$SO + OSCl \longrightarrow SCl + SO_2$	6.0×10^{-13}	Est., Mills (1998)
R335	$SO + ClSO_2 \longrightarrow OSCl + SO_2$	$5.0 \times 10^{-11}\, e^{(-800/T)}$	Estimate
R336	$SO + Na \xrightarrow{M} NaOS$	$k_0 = 1.6 \times 10^{-24}\, T^{-2}$	Est., Schofield and Steinberg (1992)
R337	$SO + NaO \longrightarrow SO_2 + Na$	6.0×10^{-11}	Estimate
R338	$SO + NaS \longrightarrow S_2O + Na$	6.0×10^{-11}	Estimate
R339	$SO + NaSO_2 \longrightarrow NaOS + SO_2$	$6.3 \times 10^{-11}\, e^{(-800/T)}$	Est. based on Schofield and Steinberg (1992)
R340	$SO_2 + Cl \xrightarrow{M} ClSO_2$	$k_0 = 1.3 \times 10^{-34}\, e^{(940/T)}$	Mills (1998)
R341	$SO_2 + ClO \longrightarrow SO_3 + Cl$	1.0×10^{-19}	Estimate
R342	$SO_2 + Na \xrightarrow{M} NaSO_2$	$k_0 = 1.58 \times 10^{-23}\, T^{-2}$	Est. based on Shi and Marshall (1991)
R343	$SO_2 + NaO \longrightarrow SO_3 + Na$	1.0×10^{-19}	Estimate
R344	$SO_2 + K \xrightarrow{M} KSO_2$	$k_0 = 4.4 \times 10^{-23}\, T^{-2}$	Est. based on Goumri *et al*. (1993)
R347	$2\ Cl \xrightarrow{M} Cl_2$	$k_0 = 3.45 \times 10^{-33}\, e^{(820/T)}$	Baulch *et al*. (1981)

TABLE A2—*Continued*

	Reaction[a]	Rate constant[b]	Reference
R348	$Cl + ClO \xrightarrow{M} Cl_2O$	$k_0 = 1.0 \times 10^{-26}\, T^{-2}$	Estimate
R351	$Cl + ClOO \longrightarrow Cl_2 + O_2$	2.3×10^{-10}	DeMore *et al*. (1997)
R352	$Cl + ClOO \longrightarrow 2\ ClO$	1.2×10^{-11}	DeMore *et al*. (1997)
R353	$Cl + OClO \longrightarrow 2\ ClO$	$3.4 \times 10^{-11}\, e^{(160/T)}$	DeMore *et al*. (1997)
R354	$Cl + Cl_2O \longrightarrow Cl_2 + ClO$	$6.2 \times 10^{-11}\, e^{(130/T)}$	DeMore *et al*. (1997)
R355	$Cl + Cl_2O_2 \longrightarrow Cl_2 + ClOO$	1.0×10^{-10}	Atkinson *et al*. (1997)
R357	$Cl + SCl \xrightarrow{M} SCl_2$	$k_0 = 1.0 \times 10^{-30}$	Est., Mills (1998)
R358	$Cl + S_2Cl \longrightarrow S_2 + Cl_2$	1.0×10^{-12}	Estimate
R359	$Cl + S_2Cl_2 \longrightarrow S_2Cl + Cl_2$	1.0×10^{-12}	Est. based on Krasnoperov *et al*. (1984)
R360	$Cl + OSCl \longrightarrow SO + Cl_2$	3.0×10^{-11}	Estimate
R361	$Cl + ClSO_2 \xrightarrow{M} SO_2Cl_2$	$k_0 = 1.0 \times 10^{-23}\, T^{-2}$	Est. based on Goumri *et al*. (1993)
R362	$Cl + ClSO_2 \longrightarrow SO_2 + Cl_2$	1.0×10^{-20}	Estimate
R363	$Cl + SO_2Cl_2 \longrightarrow ClSO_2 + Cl_2$	$1.0 \times 10^{-11}\, e^{(-1000/T)}$	Estimate
R364	$Cl + Na \xrightarrow{M} NaCl$	$k_0 = 3.0 \times 10^{-28}\, T^{-1}$	Est., Jensen and Jones (1978)
R365	$Cl + Na_2 \longrightarrow NaCl + Na$	$1.0 \times 10^{-10}\, e^{(-1000/T)}$	Estimate
R368	$Cl + NaO \longrightarrow NaCl + O$	2.0×10^{-10}	Estimate
R369	$Cl + NaO_2 \longrightarrow NaCl + O_2$	$5.0 \times 10^{-10}\, e^{(-700/T)}$	Est. based on $O + NaO_2$
R370	$Cl + Na_2O \longrightarrow NaCl + NaO$	$5.0 \times 10^{-11}\, e^{(-500/T)}$	Estimate
R372	$Cl + NaS \longrightarrow NaCl + S$	2.0×10^{-10}	Estimate
R373	$Cl + NaS_2 \longrightarrow NaCl + S_2$	$5.0 \times 10^{-10}\, e^{(-700/T)}$	Est. based on $O + NaO_2$
R374	$Cl + Na_2S \longrightarrow NaCl + NaS$	$5.0 \times 10^{-11}\, e^{(-500/T)}$	Estimate
R376	$Cl + NaOS \longrightarrow NaCl + SO$	$1.0 \times 10^{-10}\, e^{(-800/T)}$	Estimate
R377	$Cl + NaSO_2 \longrightarrow NaCl + SO_2$	$1.0 \times 10^{-10}\, e^{(-800/T)}$	Estimate
R378	$Cl + K \xrightarrow{M} KCl$	$k_0 = 5.0 \times 10^{-28}\, T^{-1}$	Est., Jensen and Jones (1978)
R379	$Cl + K_2 \longrightarrow KCl + K$	$1.0 \times 10^{-10}\, e^{(-1000/T)}$	Estimate
R382	$Cl + KO \longrightarrow KCl + O$	2.0×10^{-10}	Estimate
R383	$Cl + KO_2 \longrightarrow KCl + O_2$	$5.0 \times 10^{-10}\, e^{(-700/T)}$	Est. based on $O + NaO_2$
R384	$Cl + K_2O \longrightarrow KCl + KO$	$5.0 \times 10^{-11}\, e^{(-800/T)}$	Estimate
R386	$Cl + KS \longrightarrow KCl + S$	2.0×10^{-10}	Estimate
R387	$Cl + KS_2 \longrightarrow KCl + S_2$	$5.0 \times 10^{-10}\, e^{(-700/T)}$	Est. based on $O + NaO_2$
R388	$Cl + K_2S \longrightarrow KCl + KS$	$5.0 \times 10^{-11}\, e^{(-500/T)}$	Estimate
R389	$Cl + KSO_2 \longrightarrow KCl + SO_2$	$1.0 \times 10^{-10}\, e^{(-800/T)}$	Est. based on $Cl + NaSO_2$
R390	$Cl + KNa \longrightarrow KCl + Na$	$5.0 \times 10^{-11}\, e^{(-800/T)}$	Estimate
R391	$Cl + KNa \longrightarrow NaCl + K$	$5.0 \times 10^{-11}\, e^{(-800/T)}$	Estimate
R393	$Cl_2 + SCl \longrightarrow SCl_2 + Cl$	7.0×10^{-14}	Murrells (1988a)
R394	$Cl_2 + Na \longrightarrow NaCl + Cl$	7.3×10^{-10}	DeMore *et al*. (1997)
R395	$Cl_2 + K \longrightarrow KCl + Cl$	7.3×10^{-10}	Est. based on $Cl_2 + Na$
R404	$2\ ClO \longrightarrow O_2 + Cl_2$	$1.0 \times 10^{-12}\, e^{(-1590/T)}$	DeMore *et al*. (1997)
R405	$2\ ClO \xrightarrow{M} Cl_2O_2$	$k_0 = 1.0 \times 10^{-24}\, T^{-3.1}$	DeMore *et al*. (1997)
R407	$ClO + Cl_2O \longrightarrow ClOO + Cl_2$	4.3×10^{-16}	Basco and Dogra (1971)
R408	$ClO + SCl \longrightarrow SCl_2 + O$	1.0×10^{-14}	Estimate
R409	$ClO + S_2Cl \longrightarrow OSCl + SCl$	$5.0 \times 10^{-11}\, e^{(-1000/T)}$	Estimate
R410	$ClO + Na \longrightarrow NaCl + O$	$2.0 \times 10^{-10}\, e^{(-300/T)}$	Estimate
R412	$ClO + K \longrightarrow KCl + O$	$2.0 \times 10^{-10}\, e^{(-300/T)}$	Estimate
R426	$2\ ClOO \longrightarrow Cl_2O_2 + O_2$	1.6×10^{-11}	Baer *et al*. (1991)
R427	$ClOO + SCl \longrightarrow OSCl + ClO$	$1.0 \times 10^{-11}\, e^{(-800/T)}$	Estimate
R428	$ClOO + Na \longrightarrow NaO + ClO$	5.0×10^{-11}	Estimate
R429	$ClOO + Na \longrightarrow NaCl + O_2$	1.0×10^{-11}	Estimate
R430	$ClOO + K \longrightarrow KO + ClO$	5.0×10^{-11}	Estimate
R431	$ClOO + K \longrightarrow KCl + O_2$	1.0×10^{-11}	Estimate
R434	$OClO + Na \longrightarrow NaO + ClO$	6.0×10^{-11}	Estimate
R435	$OClO + K \longrightarrow KO + ClO$	6.0×10^{-11}	Estimate
R437	$2\ Cl_2O_2 \longrightarrow 2\ Cl_2 + 2\ O_2$	1.0×10^{-20}	Est. based on Mills (1998)
R439	$2\ SCl \longrightarrow S_2 + Cl_2$	6.0×10^{-12}	Mills (1998)
R440	$2\ SCl \longrightarrow S + SCl_2$	7.4×10^{-12}	Murrells (1988a)
R441	$2\ SCl \longrightarrow S_2Cl + Cl$	5.4×10^{-11}	Mills (1998)
R442	$2\ SCl \xrightarrow{M} S_2Cl_2$	$k_0 = 4.0 \times 10^{-31}$	Est., Mills (1998)
R443	$SCl + ClSO_2 \longrightarrow SO_2 + SCl_2$	1.0×10^{-12}	Estimate
R444	$SCl + S_2Cl \longrightarrow SCl_2 + S_2$	1.0×10^{-12}	Est., Mills (1998)
R445	$SCl + Na \longrightarrow NaCl + S$	2.0×10^{-10}	Estimate

TABLE A2—*Continued*

	Reaction[a]	Rate constant[b]	Reference
R446	$SCl + Na \longrightarrow NaS + Cl$	1.0×10^{-12}	Estimate
R447	$SCl + NaS \longrightarrow S_2Cl + Na$	1.0×10^{-10}	Estimate
R448	$SCl + NaS \longrightarrow NaCl + S_2$	$1.0 \times 10^{-10}\, e^{(-400/T)}$	Estimate
R449	$SCl + K \longrightarrow KCl + S$	2.0×10^{-10}	Estimate
R450	$SCl + K \longrightarrow KS + Cl$	1.0×10^{-12}	Estimate
R451	$SCl + KS \longrightarrow S_2Cl + K$	1.0×10^{-10}	Estimate
R452	$SCl + KS \longrightarrow KCl + S_2$	$1.0 \times 10^{-10}\, e^{(-400/T)}$	Estimate
R454	$SCl_2 + Na \longrightarrow NaCl + SCl$	3.0×10^{-10}	Estimate
R455	$S_2Cl + Na \longrightarrow NaCl + S_2$	1.0×10^{-10}	Estimate
R456	$S_2Cl_2 + Na \longrightarrow NaCl + S_2Cl$	3.0×10^{-10}	Heller and Polanyi (1936)
R457	$S_2Cl_2 + K \longrightarrow KCl + S_2Cl$	3.0×10^{-10}	Estimate
R459	$OSCl + Na \longrightarrow NaCl + SO$	$1.0 \times 10^{-10}\, e^{(-400/T)}$	Estimate
R460	$OSCl + K \longrightarrow KCl + SO$	$1.0 \times 10^{-10}\, e^{(-400/T)}$	Estimate
R462	$2ClSO_2 \longrightarrow SO_2Cl_2 + SO_2$	5.0×10^{-11}	Estimate
R463	$2ClSO_2 \longrightarrow Cl_2 + 2SO_2$	5.0×10^{-13}	Estimate
R464	$ClSO_2 + Na \longrightarrow NaCl + SO_2$	1.0×10^{-11}	Estimate
R465	$ClSO_2 + K \longrightarrow KCl + SO_2$	1.0×10^{-11}	Estimate
R466	$SO_2Cl_2 + Na \longrightarrow NaCl + ClSO_2$	$5.0 \times 10^{-11}\, e^{(-1000/T)}$	Estimate
R468	$2\,Na \xrightarrow{M} Na_2$	$k_0 = 6.0 \times 10^{-28}\, T^{-2}$	Estimate
R469	$Na + NaO \xrightarrow{M} Na_2O$	$k_0 = 1.0 \times 10^{-25}\, T^{-2}$	Estimate
R470	$Na + NaS \xrightarrow{M} Na_2S$	$k_0 = 1.0 \times 10^{-25}\, T^{-2}$	Estimate
R471	$Na + NaSO_2 \longrightarrow Na_2 + SO_2$	1.0×10^{-13}	Estimate
R472	$Na + K \xrightarrow{M} KNa$	$k_0 = 6.0 \times 10^{-28}\, T^{-2}$	Estimate
R473	$Na + KO \longrightarrow NaO + K$	$1.0 \times 10^{-12}\, e^{(-1000/T)}$	Estimate
R484	$NaCl + K \longrightarrow KCl + Na$	1.0×10^{-14}	Estimate
R485	$2\,NaCl \xrightarrow{M} (NaCl)_2$	$k_0 = 1.0 \times 10^{-25}\, T^{-2}$	Estimate
R486	$NaCl + (NaCl)_2 \xrightarrow{M} (NaCl)_3$	$k_0 = 1.0 \times 10^{-25}\, T^{-2}$	Estimate
R488	$2\,K \xrightarrow{M} K_2$	$k_0 = 6.0 \times 10^{-28}\, T^{-2}$	Estimate
R489	$K + KS \xrightarrow{M} K_2S$	$k_0 = 1.0 \times 10^{-25}\, T^{-2}$	Estimate
R493	$2\,KO \longrightarrow K_2O + O$	1.0×10^{-12}	Estimate
R497	$KS + KNa \longrightarrow K_2S + Na$	$3.0 \times 10^{-11}\, e^{(-500/T)}$	Estimate
R499	$2\,KCl \xrightarrow{M} (KCl)_2$	$k_0 = 1.0 \times 10^{-25}\, T^{-2}$	Estimate
R506	$NaCl + dust \longrightarrow NaCl_{(s)}$	condensation	
R507	$NaCl_{(s)} \longrightarrow NaCl$	evaporation	
R508	$(NaCl)_2 + dust \longrightarrow NaCl_{(s)}$	condensation	
R509	$NaCl_{(s)} \longrightarrow (NaCl)_2$	evaporation	
R510	$(NaCl)_3 + dust \longrightarrow NaCl_{(s)}$	condensation	
R511	$NaCl_{(s)} \longrightarrow (NaCl)_3$	evaporation	
R512	$(NaCl)_3 + dust \longrightarrow NaCl_{(s)}$	condensation	
R513	$NaCl_{(s)} \longrightarrow (NaCl)_3$	evaporation	
R514	$KCl + dust \longrightarrow KCl_{(s)}$	condensation	
R515	$KCl_{(s)} \longrightarrow KCl$	evaporation	
R516	$(KCl)_2 + dust \longrightarrow KCl_{(s)}$	condensation	
R517	$KCl_{(s)} \longrightarrow (KCl)_2$	evaporation	

[a] M represents any third body, prod represents higher-order products. Only the most important reactions controlling the production and loss of alkali and halogen species are included in the table.

[b] Two-body rate constants are in units of $cm^3\ s^{-1}$. Low-pressure limiting rate constants for three-body reactions (k_0) are in units of $cm^6\ s^{-1}$.

atmospheric density at any altitude level (with a corresponding column density of 1.5×10^7 particles cm^{-2}). The particle radius is assumed to be fixed at 0.1 μm. The sensitivity of our results to other assumptions is discussed in Section 4.3.

ACKNOWLEDGMENTS

The Caltech/JPL KINETICS code was developed jointly by Yuk L. Yung and Mark Allen, with assistance from many people over the years. We thank Franklin P. Mills for supplying absorption and photodissociation cross sections for several molecular species, Roger V. Yelle for supplying photoabsorption cross sections and J values for S_2, Michael E. Summers for supplying the background high-density model atmosphere, and Bernard Schmitt and Yuan-Pern Lee for interesting discussions about SO_2Cl_2. Comments from the anonymous reviewers were useful and appreciated. This paper represents Contribution Number 1105 from the Lunar and Planetary Institute, which is operated by the Universities Space Research Association. Support from the NASA Planetary Atmospheres Program is gratefully acknowledged.

REFERENCES

Allen, M., Y. L. Yung, and J. W. Waters 1981. Vertical transport and photochemistry in the terrestrial mesosphere and lower thermosphere (50–120 km). *J. Geophys. Res.* **86**, 3617–3627.

Anderson, C. M., J. Corliss, F. Scherb, and A. E. Potter 1999. Eclipse egress growth of the Na I column density in the vicinity of Io. *Bull. Am. Astron. Soc.* **31**, 1165.

Atkinson, R., D. L. Baulch, R. A. Cox, R. F. Hampson, Jr., J. A. Kerr, M. J. Rossi, and J. Troe 1997. Evaluated kinetic and photochemical data for atmospheric chemistry. Supplement VI. IUPAC subcommittee on gas kinetic data evaluation for atmospheric chemistry. *J. Phys. Chem. Ref. Data* **26**, 1329–1499.

Austin, J. V., and D. B. Goldstein 1996. Direct numerical simulations of low-density atmospheric flow on Io. In *Molecular Physics and Hypersonic Flows* (M. Capitelli, Ed.), pp. 749–758. Kluwer Academic, Dordrecht/Norwell, MA.

Austin, J. V., and D. B. Goldstein 2000. Rarefied gas model of Io's sublimation-driven atmosphere. *Icarus* **148**, 370–383.

Baer, S., H. Hippler, R. Rahn, M. Siefke, N. Seitzinger, and J. Troe 1991. Thermodynamic and kinetic properties of the reaction $Cl + O_2 + M = ClOO + M$ in the range 1600-300 K and 1-1000 bar. *J. Chem. Phys.* **95**, 6463–6470.

Bagenal, F., and J. D. Sullivan 1981. Direct plasma measurements in the Io torus and inner magnetosphere of Jupiter. *J. Geophys. Res.* **86**, 8447–8466.

Bahou, M., S.-F. Chen, and Y.-P. Lee 2000. Production and infrared absorption of $ClSO_2$ in matrices. *J. Phys. Chem. A* **104**, 3613–3619.

Ballester, G. E., D. F. Strobel, H. W. Moos, and P. D. Feldman 1990. The atmospheric abundance of SO_2 on Io. *Icarus* **88**, 1–23.

Ballester, G. E., M. A. McGrath, D. F. Strobel, X. Zhu, P. D. Feldman, and H. W. Moos 1994. Detection of the SO_2 atmosphere on Io with the Hubble Space Telescope. *Icarus* **111**, 2–17.

Basco, N., and S. K. Dogra 1971. Reactions of halogen oxides studied by flash photolysis. I. The flash photolysis of chlorine dioxide. *Proc. R. Soc. London A* **323**, 29.

Baulch, D. L., J. Duxbury, S. J. Grant, and D. C. Montague 1981. *Evaluated Kinetic Data for High Temperature Reactions. Volume 4. Homogeneous Gas Phase Reactions of Halogen- and Cyanide-Containing Species.* American Chemical Society, Washington, D.C. (also *J. Phys. Chem. Ref. Data* **10**, Suppl.).

Bergstralh, J. T., D. L. Matson, and T. V. Johnson 1975. Sodium D-line emission from Io: Synoptic observations from Table Mountain Observatory. *Astrophys. J.* **195**, L131–L135.

Bouchez, A. H., M. E. Brown, and N. M. Schneider 2000. Eclipse spectroscopy of Io's atmosphere. *Icarus* **148**, 316–319.

Brown, R. A. 1974. Optical line emission from Io. In *Exploration of the Solar System* (A. Woszczyk and C. Iwaniszewska, Eds.), pp. 527–531, Reidel, Hingham, MA.

Burger, M. H., N. M. Schneider, and J. K. Wilson 1999. Galileo's close-up view of the Io sodium jet. *Geophys. Res. Lett.* **26**, 3333–3336.

Chamberlain, J. W., and D. M. Hunten. 1987. *Theory of Planetary Atmospheres: An Introduction to Their Physics and Chemistry.* Academic Press, Orlando, FL.

Cremonese, G., N. Thomas, C. Barbieri, and C. Pernechele 1992. High resolution spectra of Io's neutral sodium cloud. *Astron. Astrophys.* **256**, 286–298.

Cremonese, G., F. Marzari, N. Eccli, and G. Corrain 1998. The Io sodium cloud: Comparison between observations and numerical models. *Icarus* **131**, 138–151.

DeMore, W. B., S. P. Sander, D. M. Golden, R. F. Hampson, M. J. Kurylo, C. J. Howard, A. R. Ravishankara, C. E. Kolb, and M. J. Molina 1997. *Chemical Kinetics and Photochemical Data for Use in Stratospheric Modeling. Evaluation Number 12.* JPL Publication 97-4, Jet Propulsion Laboratory, Pasadena.

Eska, V., U. von Zahn, and J. M. C. Plane 1999. The terrestrial potassium layer (75–110 km) between 71°S and 54°N: Observations and modeling. *J. Geophys. Res.* **104**, 17,173–17,186.

Fanale, F. P., T. V. Johnson, and D. L. Matson 1974. Io: A surface evaporite deposit? *Science* **186**, 922–925.

Fanale, F. P., T. V. Johnson, and D. L. Matson 1977. Io's surface composition: Observational constraints and theoretical considerations. *Geophys. Res. Lett.* **4**, 303–306.

Fanale, F. P., W. B. Banerdt, L. S. Elson, T. V. Johnson, and R. W. Zurek 1982. Io's surface: Its phase composition and influence on Io's atmosphere and Jupiter's magnetosphere. In *Satellites of Jupiter* (D. Morrison, Ed.), pp. 756–781. Univ. of Arizona Press, Tucson.

Farmer, V. C. 1974. *The Infrared Spectra of Minerals.* Mineralogical Society, London.

Fegley, B., Jr., and M. Yu. Zolotov 2000. Chemistry of sodium, potassium, and chlorine in volcanic gases on Io. *Icarus* **148**, 193–210.

Feldman, P. D., T. B. Ake, A. F. Berman, H. W. Moos, D. J. Sahnow, D. F. Strobel, H. A. Weaver, P. R. Young, and the FUSE Solar System Team 2000. Detection of chlorine ions in the FUSE spectrum of the Io plasma torus. *Bull. Am. Astron. Soc.* **32**, 34.01.

Geissler, P. E., A. S. McEwen, W. Ip, M. J. S. Belton, T. V. Johnson, W. H. Smyth, and A. P. Ingersoll 1999. Galileo imaging of atmospheric emissions from Io. *Science* **285**, 870–874.

Goumri, A., D. Lasko, J.-D. R. Rocha, E. Francis, and P. Marshall 1993. Investigation of the gas-phase kinetics of the reaction $K + SO_2 + Ar$. *J. Phys. Chem.* **97**, 5295–5297.

Greenwood, N. N. 1970. *Ionic Crystals Lattice Defects and Nonstoichiometry.* Chemical Pub. Co., New York.

Haff, P. K., C. C. Watson, and Y. L. Yung 1981. Sputter-ejection of matter from Io. *J. Geophys. Res.* **86**, 6933–6938.

Heller, W., and M. Polanyi 1936. Reactions between sodium vapour and volatile polyhalides. Velocities and luminescences. *Trans. Farad. Soc.* **32**, 633.

Helmer, M., and J. M. C. Plane 1993. A study of the reaction $NaO_2 + O \rightarrow NaO + O_2$: Implications for the chemistry of sodium in the upper atmosphere. *J. Geophys. Res.* **98**, 23,207–23,222.

Hendrix, A. R., C. A. Barth, and C. W. Hord 1999. Io's patchy atmosphere as measured by the Galileo Ultraviolet Spectrometer. *J. Geophys. Res.* **104**, 11,817–11,826.

Ingersoll, A. P. 1989. Io meteorology: How atmospheric pressure is controlled locally by volcanos and surface frosts. *Icarus* **81**, 298–313.

Jensen, D. E., and G. A. Jones 1978. Reaction rate coefficients for flame calculations. *Combust. Flame* **32**, 1–34.

Johnson, R. E. 1994. Formation of Na-containing molecular ions at Io. *Icarus* **111**, 65–72.

Kittel, C. 1976. *Introduction to Solid State Physics.* Wiley, New York.

Krasnoperov, L. N., E. N. Chesnokov, and V. N. Panfilov 1984. Application of laser magnetic resonance with time resolution to the measurement of the rates of elementary reactions of the Cl atom and SiH_3 radical during the flash photolysis of S_2Cl_2 in the presence of SiH_4. *Dokl. Phys. Chem.* (Engl. Transl.) **277**, 636–640.

Kumar, S. 1980. A model of the SO_2 atmosphere and ionosphere of Io. *Geophys. Res. Lett.* **7**, 9–12.

Kumar, S. 1982. Photochemistry of SO_2 in the atmosphere of Io and implications on atmospheric escape. *J. Geophys. Res.* **87**, 1677–1684.

Kumar, S. 1984. Sulfur and oxygen escape from Io and a lower limit to atmospheric SO_2 at Voyager 1 encounter. *J. Geophys. Res.* **89**, 7399–7406.

Kumar, S. 1985. The SO_2 atmosphere and ionosphere of Io: Ion chemistry, atmospheric escape, and models corresponding to the Pioneer 10 radio occultation measurements. *Icarus* **61**, 101–123.

Küppers, M., and N. M. Schneider 2000. Discovery of chlorine in the Io Torus. *Geophys. Res. Lett.* **27**, 513–516.

Lellouch, E. 1996. Io's atmosphere: Not yet understood (Urey Prize lecture). *Icarus* **124**, 1–21.

Lellouch, E., M. Belton, I. de Pater, S. Gulkis, and T. Encrenaz 1990. Io's atmosphere from microwave detection of SO_2. *Nature* **346**, 639–641.

Lellouch, E., M. Belton, I. de Pater, G. Paubert, S. Gulkis, and T. Encrenaz 1992. The structure, stability, and global distribution of Io's atmosphere. *Icarus* **98**, 271–295.

Lellouch, E., D. Strobel, M. Belton, G. Paubert, G. Ballester, and I. de Pater 1994. Millimeter wave observations of Io's atmosphere: new data and new models. *Bull. Am. Astron. Soc.* **26**, 1136.

Lellouch, E., D. F. Strobel, M. J. S. Belton, M. E. Summers, G. Paubert, and R. Moreno 1996. Detection of sulfur monoxide in Io's atmosphere. *Astrophys. J.* **459**, L107–L110.

Mallard, W. G., Y. Mirokhin, F. Westley, J. T. Herron, R. F. Hampson, and D. H. Frizzell 1998. *NIST Chemical Kinetics Database 17-2Q98*. National Inst. Standards and Tech., Gaithersburg, MD.

Matson, D. L., and D. B. Nash 1983. Io's atmosphere: Pressure control by regolith cold trapping and surface venting. *J. Geophys. Res.* **88**, 4771–4783.

Matson, D. L., T. V. Johnson, and F. P. Fanale 1974. Sodium D-line emission from Io: Sputtering and resonant scattering hypotheses. *Astrophys. J.* **192**, L43–L46.

McEwen, A. S., and L. A. Soderblom 1983. Two classes of volcanic plumes on Io. *Icarus* **55**, 191–217.

McEwen, A. S., L. Keszthelyi, P. Geissler, D. P. Simonelli, M. H. Carr, T. V. Johnson, K. P. Klaasen, H. H. Breneman, T. J. Jones, J. M. Kaufman, K. P. Magee, D. A. Senske, M. J. S. Belton, and G. Schubert 1998. Active volcanism on Io as seen by Galileo SSI. *Icarus* **135**, 181–219.

McEwen, A. S., and 25 colleagues 2000. Galileo at Io: Results from high-resolution imaging. *Science* **288**, 1193–1198.

McGrath, M. A., and R. E. Johnson 1987. Magnetospheric plasma sputtering of Io's atmosphere. *Icarus* **69**, 519–531.

McGrath, M. A., M. J. S. Belton, J. R. Spencer, and P. Sartoretti 2000. Spatially resolved spectroscopy of Io's Pele plume and SO_2 atmosphere. *Icarus* **146**, 476–493.

Mendillo, M., J. Baumgardner, B. Flynn, and W. J. Hughes 1990. The extended sodium nebula of Jupiter. *Nature* **348**, 312–314.

Mendillo, M., J. K. Wilson, J. Baumgardner, N. M. Schneider, J. Spencer, J. Stansberry, B. Flynn, and J. T. Trauger 1999. The relationship between Io's sodium clouds and volcanic activity on Io. *Bull. Am. Astron. Soc.* **31**, 1165.

Mills, F. P. 1998. *I. Observations and Photochemical Modeling of the Venus Middle Atmosphere. II. Thermal Infrared Spectroscopy of Europa and Callisto*. Ph.D. thesis, California Institute of Technology, Pasadena, CA.

Moreno, M. A., G. Schubert, J. Baumgardner, M. G. Kivelson, and D. A. Paige 1991. Io's volcanic and sublimation atmospheres. *Icarus* **93**, 63–81.

Moses, J. I., E. Lellouch, B. Bézard, G. R. Gladstone, H. Feuchtgruber, and M. Allen 2000. Photochemistry of Saturn's atmosphere. II. Effects of an influx of external oxygen. *Icarus* **145**, 166–202.

Moses, J. I., M. Yu. Zolotov, and B. Fegley, Jr. 2002. Photochemistry of a volcanically driven atmosphere on Io: Sulfur and oxygen species from a Pele-type eruption. *Icarus* **156**, 76–106.

Murcray, F. J., and R. Goody 1978. Pictures of the Io sodium cloud. *Astrophys. J.* **226**, 327–335.

Murrells, T. P. 1988a. Elementary reactions of the SCl radical. Part I. Rate constants and mechanisms of the reactions $Cl + C_2H_4S \rightarrow SCl + C_2H_4$, $SCl +$ $SCl \rightarrow$ products and $SCl + Cl_2 \rightarrow SCl_2 + Cl$. *J. Chem. Soc. Faraday Trans. 2* **84**, 67–84.

Murrells, T. P. 1988b. Elementary reactions of the SCl radical. Part II. Rate constants and mechanisms of the reactions of SCl with NO_2, NO, O_2, $O(^3P)$, and $N(^4S)$. *J. Chem. Soc. Faraday Trans. 2* **84**, 85–94.

Nash, D. B., and F. P. Fanale 1977. Io's surface composition based on reflectance spectra of sulfur/salt mixtures and proton-irradiated experiments. *Icarus* **31**, 40–80.

Nelson, R. M., and B. W. Hapke 1978. Spectral reflectivities of the Galilean satellites an Titan, 0.32 to 0.86 micrometers. *Icarus* **36**, 304–329.

Pilcher, C. B., W. H. Smyth, M. R. Combi, and J. H. Fertel 1984. Io's sodium directional features: Evidence for a magnetospheric-wind-driven gas escape mechanism. *Astrophys. J.* **287**, 427–444.

Plane, J. M. C., and M. Helmer 1994. Laboratory studies of the chemistry of meteoric metals. In *Research in Chemical Kinetics* (R. G. Compton and G. Hancock, Eds.), Vol. 2, pp. 313–367, Elsevier, New York.

Plane, J. M. C., and D. Husain 1986. Determination of the absolute rate constant for the reaction $O + NaO \rightarrow Na + O_2$ by time-resolved atomic chemiluminescence at $\lambda = 589$ nm $[Na(3^2P_J) \rightarrow Na(3^2S_{1/2}) + h\nu]$. *J. Chem. Soc. Faraday Trans. 2* **82**, 2047–2052.

Plane, J. M. C., C.-F. Nien, M. R. Allen, and M. Helmer 1993. A kinetic investigation of the reactions $Na + O_3$ and $NaO + O_3$ over the temperature range 207–377 K. *J. Phys. Chem.* **97**, 4459–4467.

Pospieszalska, M. K., and R. E. Johnson 1992. Plasma heating of Io's atmosphere. *Geophys. Res. Lett.* **19**, 949–952.

Rajasekhar, B., J. M. C. Plane, and Libero Bartolotti 1989. Determination of the absolute photolysis cross section of sodium superoxide at 230 K: Evidence for the formation of sodium tetroxide in the gas phase. *J. Phys. Chem.* **93**, 7399–7404.

Retherford, K. D., P. D. Feldman, H. W. Moos, D. F. Strobel, B. C. Wolven, R. J. Oliversen, M. A. McGrath, F. L. Roesler, F. Scherb, G. E. Ballester, W. H. Smyth, and F. Bagenal 2000. Io's UV aurora: Detection of neutral hydrogen and neutral chlorine. *Bull. Am. Astron. Soc.* **32**, 34.06.

Roesler, F. L., H. W. Moos, R. J. Oliversen, R. C. Woodward, Jr., K. D. Retherford, F. Scherb, M. A. McGrath, W. H. Smyth, P. D. Feldman, and D. F. Strobel 1999. Far-ultraviolet imaging spectroscopy of Io's atmosphere with HST/STIS. *Science* **283**, 353–357.

Sartoretti, P., M. A. McGrath, and F. Paresce 1994. Disk-resolved imaging of Io with the Hubble Space Telescope. *Icarus* **108**, 272–284.

Sartoretti, P., M. J. S. Belton, and M. A. McGrath 1996. SO_2 distributions on Io. *Icarus* **122**, 273–287.

Scherb, F., and W. H. Smyth 1993. Variability of [O I] 6300 Å emission near Io. *J. Geophys. Res.* **98**, 18,729–18,736.

Schmitt, B., and S. Rodriguez 2000. Tentative identification of a chlorine molecule at Io's surface. *Bull. Am. Astron. Soc.* **32**, 29.10.

Schmitt, B., S. Rodriguez, and the NIMS Team 2001. Tentative identification of local deposits of Cl_2SO_2 at Io's surface. *Lunar Planet. Sci.* **32**, 1710.

Schneider, N. M., W. H. Smyth, and M. A. McGrath 1989. Io's atmosphere and neutral clouds. In *Time-Variable Phenomena in the Jovian System* (M. J. S. Belton, R. A. West, and J. Rahe, Eds.), pp. 75–99, NASA SP-494, Washington, DC.

Schneider, N. M., D. M. Hunten, W. K. Wells, A. B. Schultz, and U. Fink 1991a. The structure of Io's corona. *Astrophys. J.* **368**, 298–315.

Schneider, N. M., J. T. Trauger, J. K. Wilson, D. I. Brown, R. W. Evans, and D. E. Shemansky 1991b. Molecular origin of Io's fast sodium. *Science* **253**, 1394–1397.

Schneider, N. M., A. H. Park, and M. E. Kuppers 2000. Spectroscopic studies of the Io torus during Galileo encounters: Remote plasma diagnostics and the detection of Cl^{++}. *Bull. Am. Astron. Soc.* **32**, 35.03.

Schofield, K., and M. Steinberg 1992. Sodium/sulfur chemical behavior in fuel-rich and -lean flames. *J. Phys. Chem* **96**, 715–726.

Shi, Y., and P. Marshall 1991. A kinetic study of the recombination reaction $Na + SO_2 + Ar$. *J. Phys. Chem.* **95**, 1654–1658.

Sieveka, E. M., and R. E. Johnson 1984. Ejection of atoms and molecules from Io by plasma-ion impact. *Astrophys. J.* **287**, 418–426.

Sieveka, E. M., and R. E. Johnson 1985. Nonisotropic coronal atmosphere on Io. *J. Geophys. Res.* **90**, 5327–5331.

Silver, J. A., D. R. Worsnop, A. Freedman, and C. E. Kolb 1986. Absolute photodissociation cross sections of gas phase sodium chloride at room temperature. *J. Chem. Phys.* **84**, 4378–4384.

Smyth, W. H., and M. R. Combi 1988. A general model for Io's neutral gas clouds. II. Application to the sodium cloud. *Astrophys. J.* **328**, 888–918.

Smyth, W. H., and M. R. Combi 1991. The sodium zenocorona. *J. Geophys. Res.* **96**, 22,711–22,727.

Smyth, W. H., and M. R. Combi 1997. Io's sodium corona and spatially extended cloud: A consistent flux speed distribution. *Icarus* **126**, 58–77.

Spencer, J. R., and N. M. Schneider 1996. Io on the eve of the Galileo mission. *Ann. Rev. Earth Planet. Sci.* **24**, 125–190.

Spencer, J. R., K. L. Jessup, M. A. McGrath, G. E. Ballester, and R. Yelle 2000. Discovery of gaseous S_2 in Io's Pele plume. *Science* **288**, 1208–1210.

Strobel, D. F., and B. C. Wolven 2001. The atmosphere of Io: Abundances and sources of sulfur dioxide and atomic hydrogen. *Astrophys. Space Sci.* **277**, 271–287.

Strobel, D. F., X. Zhu, and M. E. Summers 1994. On the vertical thermal structure of Io's atmosphere. *Icarus* **111**, 18–30.

Summers, M. E. 1985. *Theoretical Studies of Io's Atmosphere.* Ph.D. thesis, California Institute of Technology, Pasadena, CA.

Summers, M. E., and D. F. Strobel 1996. Photochemistry and vertical transport in Io's atmosphere and ionosphere. *Icarus* **120**, 290–316.

Thomas, N. 1992. Optical observations of Io's neutral clouds and plasma torus. *Surveys Geophys.* **13**, 91–164.

Trafton, L. 1975. Detection of a potassium cloud near Io. *Nature* **258**, 690–692.

Trafton, L. 2000. Search for proton aurora and ambient hydrogen on Io. *Astron. J.* **120**, 488–495.

Trafton, L., T. Parkinson, and W. Macy 1974. The spatial extent of sodium emission around Io. *Astrophys. J.* **190**, L85–L89.

Wilson, J. K., and N. M. Schneider 1994. Io's fast sodium: Implications for molecular and atomic atmospheric escape. *Icarus* **111**, 31–44.

Wilson, J. K., and N. M. Schneider 1999. Io's sodium directional feature: Evidence for ionospheric escape. *J. Geophys. Res.* **104**, 16,567–16,583.

Wong, M. C., and R. E. Johnson 1996a. A three-dimensional azimuthally symmetric model atmosphere for Io. 1. Photochemistry and the accumulation of a nightside atmosphere. *J. Geophys. Res.* **101**, 23,243–23,254.

Wong, M. C., and R. E. Johnson 1996b. A three-dimensional azimuthally symmetric model atmosphere for Io. 2. Plasma effect on the surface. *J. Geophys. Res.* **101**, 23,255–23,259.

Wong, M. C., and W. H. Smyth 2000. Model calculations for Io's atmosphere at eastern and western elongations. *Icarus* **146**, 60–74.

Yung, Y. L., M. Allen, and J. P. Pinto 1984. Photochemistry of the atmosphere of Titan: Comparison between model and observations. *Astrophys. J. Suppl. Ser.* **55**, 465–506.

Zolotov, M. Yu., and B. Fegley, Jr. 1998a. Volcanic origin of disulfur monoxide (S_2O) on Io. *Icarus* **133**, 293–297.

Zolotov, M. Yu., and B. Fegley, Jr. 1998b. Volcanic production of sulfur monoxide (SO) on Io. *Icarus* **132**, 431–434.

Zolotov, M. Yu., and B. Fegley, Jr. 1999. Oxidation state of volcanic gases and the interior of Io. *Icarus* **141**, 40–52.

Zolotov, M. Yu., and B. Fegley, Jr. 2000. Eruption conditions of Pele volcano on Io inferred from chemistry of its volcanic plume. *Geophys. Res. Lett.* **27**, 2789–2792.